PNAS RESEARCH ARTICLE | MICROBIOLOGY

Signal integration in chemoreceptor complexes

Moriah Koler[a], John S. Parkinson[b], and Ady Vaknin[a,1]

Edited by Caroline Harwood, University of Washington, Seattle, WA; received July 15, 2023; accepted March 1, 2024

Motile bacteria use large receptor arrays to detect chemical and physical stimuli in their environment, process this complex information, and accordingly bias their swimming in a direction they deem favorable. The chemoreceptor molecules form tripod-like trimers of receptor dimers through direct contacts between their cytoplasmic tips. A pair of trimers, together with a dedicated kinase enzyme, form a core signaling complex. Hundreds of core complexes network to form extended arrays. While considerable progress has been made in revealing the hierarchical structure of the array, the molecular properties underlying signal processing in these structures remain largely unclear. Here we analyzed the signaling properties of nonnetworked core complexes in live cells by following both conformational and kinase control responses to attractant stimuli and to output-biasing lesions at various locations in the receptor molecule. Contrary to the prevailing view that individual receptors are binary two-state devices, we demonstrate that conformational coupling between the ligand binding and the kinase-control receptor domains is, in fact, only moderate. In addition, we demonstrate communication between neighboring receptors through their trimer-contact domains that biases them to adopt similar signaling states. Taken together, these data suggest a view of signaling in receptor trimers that allows significant signal integration to occur within individual core complexes.

chemotaxis | cell signaling | receptor array | signal integration

Significance

The ability of motile bacteria to navigate their environments influences many aspects of their life. This behavior relies on sensory receptor arrays that detect and process complex chemical and physical information about the environment to produce movements in beneficial directions. The molecular properties that govern signal processing in bacterial chemoreceptor arrays remain largely unclear. By employing a mutation that disrupts the networking of receptor signaling complexes, we could study their intrinsic signaling properties in live cells. We show that signals detected by different receptors first interact within the core signaling units that comprise the extended array. Our findings suggest that signaling interactions between core-complex receptors could have significant impact on overall signal integration in receptor arrays.

Chemotactic behaviors—the adaptive movements of motile organisms in chemical gradients—influence many aspects of bacterial life, including assembly of microbial communities and the process of host invasion (1). In each bacterial cell, large receptor arrays sense and process complex chemical and physical information about the environment and compute whether the cell is heading in a favorable direction. This sensory information enables the bacterial cell to modulate internal signals that control its locomotor behavior.

The bacterium *Escherichia coli*, a well-established model organism for studying bacterial chemotaxis (2), has five representatives of the methyl-accepting chemotaxis protein (MCP) receptor superfamily (3, 4). Its two principal chemoreceptors are the serine (Tsr) and aspartate (Tar) sensors, which operate as long (~40 nm), predominantly alpha-helical, transmembrane homodimers. Their cytoplasmic signaling domains are highly conserved, with an invariant hairpin tip that contains interaction surfaces that assemble core complexes (Fig. 1*A*), the basic receptor signaling unit. Homodimeric receptor molecules interact at their tips to form trimers of dimers that may contain members with different detection specificities (5, 6). Two receptor trimers, through binding interactions with an adapter protein (CheW), share a homodimeric histidine kinase (CheA) to form core complexes that activate and modulate CheA autophosphorylation (7, 8). Binding interactions between core units, through the interface 2 surfaces of CheW and the CheA.P5 domain (Fig. 1 *A*, *Top* view), network core complexes into extended arrays (9–11) that exhibit highly cooperative signaling behavior (9), thus enhancing detection sensitivity, dynamic range, and chemotaxis efficiency (12–17).

Ligand-binding signals detected by the periplasmic sensing domain of the receptors propagate through a series of signaling elements (Fig. 1*B*), including the HAMP domain, the methylation-helix (MH) bundle, and a flexible region encompassing a glycine hinge, to reach the kinase-controlling hairpin tip (4). Active CheA autophosphorylates its P1 domain that, in turn, donates the phosphoryl groups to the CheY response regulator (Fig. 1*A*). The action of a dedicated phosphatase CheZ renders the phospho-CheY short-lived, allowing it to follow rapid changes in the external signals and accordingly modulate the rotation of the flagellar motors, which, in turn, control the swimming behavior of the bacteria (18).

The signaling states of the chemoreceptors adapt to a steady input signal through activity-dependent reversible modifications at 4 (Tar) or 5 (Tsr) specific glutamyl (E) residues in the sensory adaptation region of the MH bundle (Fig. 1*B*) (19–21). Methyltransferase CheR acts on OFF-state receptors promoting methylation and shifting their output toward the kinase-ON state. Methylesterase CheB acts on ON-state receptors promoting demethylation and shifting their output toward the kinase-OFF state. In the wild-type Tsr and Tar

Author affiliations: [a]The Racah Institute of Physics, The Hebrew University, Jerusalem 91904, Israel; and [b]School of Biological Sciences, University of Utah, Salt Lake City, UT 84112

Author contributions: J.S.P. and A.V. designed research; M.K. and A.V. performed research; M.K. and J.S.P. contributed new reagents/analytic tools; A.V. analyzed data; and J.S.P. and A.V. wrote the paper.

The authors declare no competing interest.

This article is a PNAS Direct Submission.

[1]To whom correspondence may be addressed. Email: avaknin@mail.huji.ac.il.

This article contains supporting information online at https://www.pnas.org/lookup/suppl/doi:10.1073/pnas.2312064121/-/DCSupplemental.

Published March 26, 2024.

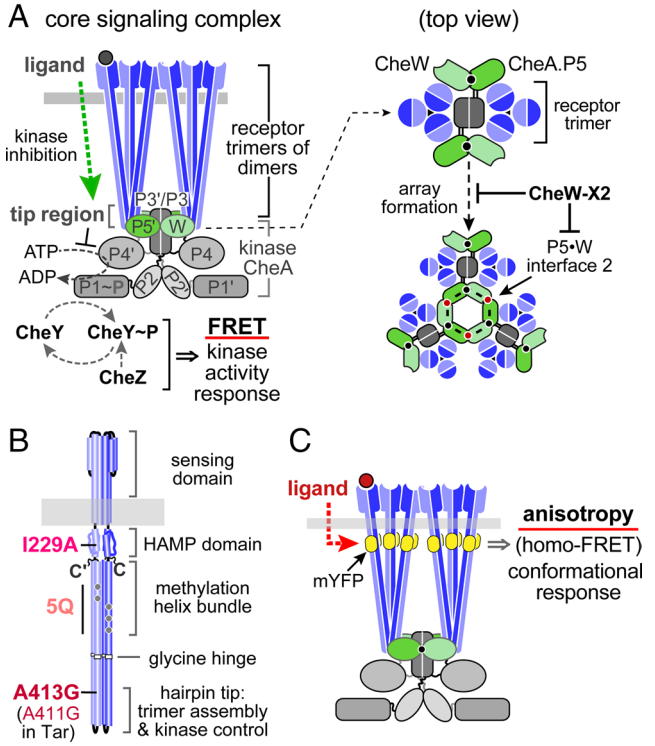

Fig. 1. The receptor core complex and two assays for monitoring its ligand response. (*A*) Schematic of the core complex, which consists of two receptor trimers of dimers, one CheA dimer, and two protomers of the CheW scaffolding protein. Binding of an attractant ligand to the periplasmic sensing domain of a receptor initiates conformational changes that propagate to the cytoplasmic tip region to modulate the CheA autokinase activity, which we followed with an in vivo CheY/CheZ FRET assay (*Materials and Methods*). The top–down cross-section view of the tip region of the core complex (on the *Right*) shows the interface 1 interactions (black circles) between CheW and the P5 domain of CheA that are critical to core complex assembly and operation. A second CheW-CheA.P5 interaction, interface 2 (red circles), networks core units into an extended signaling array. The CheW interface 2 lesion (CheW-X2) prevents array assembly and permits study of signaling events in nonnetworked core units. (*B*) Signaling architecture of the receptor dimer and the positions of locked-ON Tsr lesions used here. (*C*) The fluorescence anisotropy (homo-FRET) assay of signaling responses (*Materials and Methods*). The mYFP-tag is positioned at the C termini of the receptor protomers. Ligand binding induces conformational changes in the complex that modulate packing of the fluorescent tags and their homo-FRET interactions, leading to changes in the polarization (anisotropy) of their emitted light upon excitation with plane polarized light.

receptors, two of the methyl-accepting sites are initially translated as glutamines (labeled QEQE), which mimic the signaling properties of glutamyl methyl esters. Those Q residues are irreversibly converted to E residues through the deamidation activity of CheB. The E sites then undergo CheR and CheB modifications that shift the conformational bias of the receptor to offset the effects of ligands. The opposing actions and substrate preferences of these two enzymes provide for integral feedback control of receptor sensitivity. The methylation status of the receptors serves as a record of their recent activity history and thus enables the cell to detect temporal changes in chemoeffector levels along its trajectory over a wide range of chemoeffector concentrations (12, 22, 23). If the cell deems the gradient along its trajectory attractive, the receptor arrays inhibit the total kinase activity thereby promoting counterclockwise rotation of the flagellar motors and an up-gradient swimming bias.

Chemoreceptor molecules have long been considered to operate as two-state signaling devices with discrete conformations that respectively correspond to the ligand-bound (kinase-OFF) and unbound (kinase-ON) output states (14–16, 24, 25). This model has been extended to include dynamic behavior and conformational flexibility of receptor signaling complexes (26–28). These dynamic considerations may also apply to the networked array (29, 30). Dynamics-based signaling models propose that the structures of adjoining receptor elements are coupled in opposing ways, such that as one element gains structural stability, its adjacent neighbors become more dynamic. Yet, if structural coupling between successive domains were strong enough, the domains would be strictly correlated, and the receptor dimers would still function effectively as a two-state switch. However, owing to the highly cooperative signaling responses of homogeneous receptor arrays, the coupling properties within individual receptors or trimers cannot be discerned directly from the responses of the array.

Here, we sought to elucidate allosteric interactions between receptor molecules in nonnetworked core signaling complexes (Fig. 1*A*). We therefore studied the response behaviors of cells with an interface 2 lesion in the CheW protein (CheW-X2) that disrupts network connections between core complexes in the array, but retains their ability to activate and control the kinase (9, 13). To detect signaling-related conformational changes in core complexes we used two types of structural reporters. First, we inferred the signaling state of the kinase-controlling tip region of the receptors from the output kinase activity (Fig. 1*A*), detected by monitoring the association between fluorescently tagged CheY~P and CheZ using Förster resonance energy transfer (FRET) measurements (12, 31). Second, conformational changes at the upper (membrane-proximal) part of core complexes were detected by measuring fluorescence anisotropy of monomeric yellow fluorescent protein (mYFP) tags attached to the C termini of the receptors (Fig. 1*C*) (32, 33). Because the fluorophore in mYFP is anchored to the protein frame, it exhibits slow rotational diffusion and high fluorescence anisotropy (polarization), which makes it sensitive to homo-FRET interactions that can reduce the anisotropy. Thus, this assay reports on signaling-related conformational changes that modulate the relative distance within or between the trimers in core complexes, most likely involving bending or tilting of the receptor dimers. Both attractant stimuli and low receptor modification state shift kinase output toward the OFF state and also increase the fluorescence anisotropy (32). Notably, unlike the anisotropy responses of receptor arrays that include a slow-evolving component (29), the anisotropy responses of nonnetworked core complexes are more abrupt (9). To assess transmission of stimulus signals between the FRET kinase and anisotropy reporters, we used locked-ON lesions at different points along the receptor that trapped the tip in a kinase-active conformation (Fig. 1*B*).

Our findings suggest that individual receptors do not act as binary two-state devices, but rather that conformational communication between receptor structural elements occurs through moderate coupling strengths that can lead to different signaling behaviors in different parts of the receptor molecule. Furthermore, the data demonstrate communication between receptor dimers in core complexes through their tip domains. Based on these observations, we suggest a view of receptor signaling in which the trimer tip serves as the first point where signals communicated through different receptors can be effectively integrated.

Results

Moderate Coupling between the Receptor Upper Signaling Domains and the Kinase-Controlling Tip Domain. If receptor dimers operate as a global two-state switch (Fig. 1*B*), strong coupling between their signaling elements would ensure that a signaling shift in one domain would trigger a global shift in the receptor signaling state. To test this view, we first identified structural changes at various locations along the Tsr receptor (Fig. 1*B*) that

locked its kinase-controlling tip domain in the kinase-ON state. Subsequently, we examined whether ligand binding in these mutant receptors could still induce conformational changes at the upper (membrane-proximal) part of core complexes, detected by fluorescence anisotropy (Fig. 1*C*). These measurements were done in strain VF7 cells [ΔMCPs, Δ(*cheRBYZ), cheW-X2*], a derivative of *E. coli* K-12 strain RP437 (34) with an interface 2 lesion in the CheW protein that disrupts network connections between core complexes (Fig. 1*A*).

The signaling state of the kinase-controlling tip domain was inferred from measurements of the kinase output using spectral-shift FRET between mCherry-tagged CheY and mYFP-tagged CheZ-F98S (Fig. 1*A* and *Materials and Methods*). To control for any structural perturbation that might be caused by the mYFP tag used in the anisotropy measurements, we ensured that both the anisotropy and the CheY-Z FRET measurements were conducted with similar complexes by introducing a similar (monomeric cyan fluorescent protein, mCFP) tag at the C termini of the receptors for the CheY-Z FRET measurements. Note that the mCFP tag does not interfere with the FRET measurements. Because ligands fail to inhibit the kinase output of locked-ON receptor complexes, we used a sodium cyanide (NaCN) "stimulus" to assess their kinase activity. NaCN collapses cellular ATP level and thus blocks ATP-dependent kinase CheA activity (35).

A sample trace of the mCherry/mYFP fluorescence ratio is shown in Fig. 2 *A*, *Left* for the Tsr [QQQQ]-E502Q receptor that has methyl-mimicking glutamine residues at all five modification sites (a 5Q receptor). Three principal levels of kinase activity were apparent (Fig. 2 *A*, *Left*): the no-ligand activity, a slightly lower ligand-bound activity, and the much lower kinase-off NaCN baseline. In contrast, serine produced complete inhibition of kinase activity in the parental Tsr [QQQQE] receptor (*Inset*). Notably, the E502Q lesion led to clearer locked-ON behavior in the Tsr [QQQQE] background, compared with Tsr [QEQEE], suggesting that all the five Q replacements contribute to its locked-ON phenotype. The ratio between the ligand-bound ("+ligand") and the no-ligand kinase-activity levels for the different receptor variants is plotted on the *Right* part of Fig. 2*A* (see *SI Appendix*, Fig. S1 for additional data). Note that lesions other than E502Q were made in a QEQEE background. In addition to Tsr (5Q), the A413G and A411G lesions near the hairpin tips of Tsr and Tar, respectively, and the I229A lesion in the Tsr HAMP domain also exhibited locked-ON kinase output, indicating that the kinase-controlling tip domains in these receptor complexes remain in the ON conformation regardless of their ligand binding state.

We then assessed ligand-induced conformational changes in the membrane-proximal part of core complexes by measuring fluorescence anisotropy (*r*) of mYFP tags at the C termini of the receptors (Fig. 1*C* and *Materials and Methods*) (32, 33, 36). For a better defined structure near the mYFP (or mCFP) tags, the fluorescence tag was added to the receptor while omitting the flexible linker (521+ in Tsr or 528+ in Tar) (32, 33), as it is not essential for ligand-induced kinase control (37). Sample anisotropy responses of mutant (colored symbols) and parental receptors (gray symbols) are shown in Fig. 2 *B*, *Left* plots. Additional responses are shown in *SI Appendix*, Fig. S2. The ratio of the anisotropy response amplitude between the various receptor mutants and their parental receptors are shown in the *Right* plot. Clearly, Tsr-I229A and Tsr [QQQQ]-E502Q had modest conformational responses to serine stimuli. However, Tsr-A413G and Tar-A411G, despite their locked-ON kinase behavior demonstrated in Fig. 2*A*, showed substantial conformational responses of their membrane-proximal signaling domains to their respective ligands (Fig. 2*B*). Notably, the anisotropy dose–response behaviors of these mutant receptor

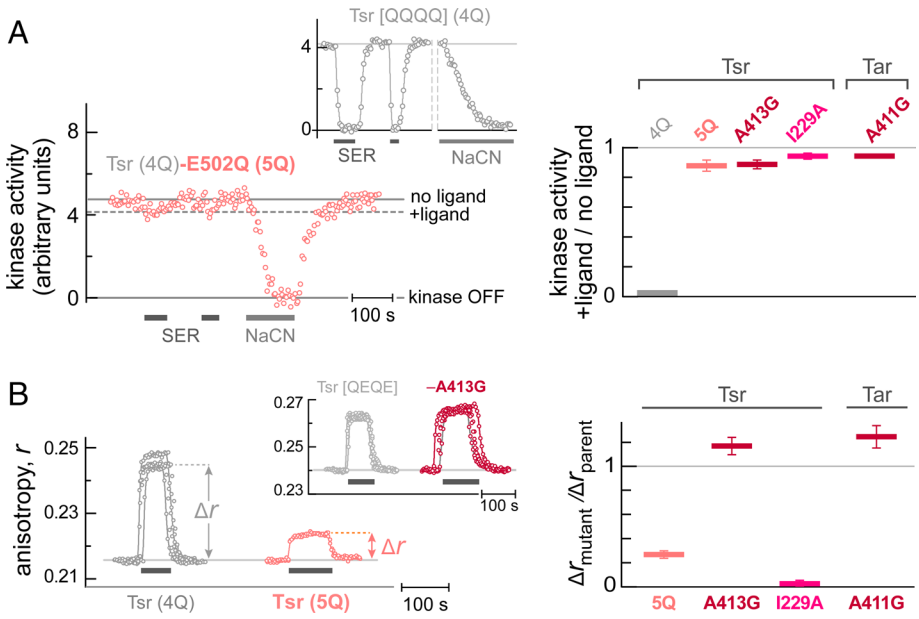

Fig. 2. Signaling behaviors of mutant Tsr and Tar receptors. (*A*) Receptor-controlled kinase responses (Fig. 1*A* and *Materials and Methods*). (*Left*) Fluorescence-ratio traces (CheY-mCherry/CheZ-mYFP) of VF7 cells (CheW-X2) expressing Tsr (4Q) (*Inset*), with methyl-mimicking Q residues at adaptation sites 1 to 4, or Tsr (5Q) [Tsr (4Q) carrying the ON-shifting E502Q lesion]. Cells were challenged with serine (SER; 10 mM) and NaCN (3 mM) during the periods indicated by the horizontal bars. (*Right*) For each receptor variant, the kinase activity in the presence of ligand (10 mM serine for Tsr or 10 mM MeAsp for Tar) is plotted and normalized by the corresponding no-ligand activity. Error bars represent additional data shown in *SI Appendix*, Fig. S1. Receptor variants were tagged with mCFP, which does not interfere with the FRET measurements (see text). (*B*) Ligand-induced conformational (anisotropy) responses (Fig. 1*C* and *Materials and Methods*). (*Left*) Two examples of anisotropy (*r*) responses in VF7 cells carrying mYFP-tagged parental receptors or their mutant derivatives: Tsr-mYFP (4Q) vs. (5Q) (main plot) and Tsr-mYFP [QEQE] vs. A413G (*Inset*). Cells were challenged with serine (10 mM) during the periods indicated by the horizontal bars. To allow for direct comparison, the entire traces of the mutant receptors were shifted upward (*SI Appendix*, Fig. S2). The cells also carried an empty pKG110 vector to control for the pKG110 derivative that supplied the FRET reporter pair in (*A*). (*Right*) Summary of ligand-induced anisotropy responses. For each receptor mutant, the response amplitude was normalized by the corresponding response amplitude of the parental receptors. Error bars represent additional data shown in *SI Appendix*, Fig. S2.

complexes were shifted toward higher ligand concentrations (*SI Appendix*, Fig. S3), reflecting an expected coupling between the receptor tip and upper (membrane-proximal) domains. However, this structural coupling was moderate in that ligand binding was able to trigger a conformational response at the upper part of the receptor despite having a locked-ON output conformation at the hairpin tip.

Evidence for Coupling between Neighboring Receptor Tips. Conformational coupling between neighboring receptors in core complexes could potentially result from their direct contacts at the trimer contact region near the receptor hairpin tip (Fig. 1 *A* and *B*). To explore such coupling, we studied mixed complexes containing Tsr-mYFP and untagged Tar receptors, and asked whether the Tar receptors could affect the anisotropy responses of the Tsr-mYFP receptors to serine stimuli (Fig. 3). Indeed, we found that mixing high-activity Tar (4Q) receptors with low-activity Tsr-mYFP [QEEEE] (1Q) receptors shifted the Tsr-mYFP anisotropy response toward higher serine concentrations (Fig. 3 *A*, *Left-Middle* plot), consistent with a shift of the Tsr-mYFP (1Q) receptors toward a higher activity state. In similar experiments, done in the presence of alpha-methyl-aspartate (MeAsp), which drives Tar (4Q) receptors to the low activity state, the Tsr-mYFP (1Q) response shifted back toward lower serine concentrations (Fig. 3 *A*, *Left-Lower* plot). In contrast, mixing weakly active Tar (4E) receptors in complexes with high-activity Tsr-mYFP (4Q) receptors had no significant effect on the Tsr-mYFP (4Q) response to serine (Fig. 3 *A*, *Right-Middle* plot). However, in similar experiments, done in the presence of MeAsp, which drives Tar (4E) receptors to the low activity state, the Tsr-mYFP (4Q) response did shift toward lower serine concentrations (Fig. 3 *A*, *Right-Lower* plot), consistent with a shift of the Tsr-mYFP (4Q) receptors toward a lower activity state. Output-locking tip lesions in Tsr-mYFP abolished its Tar-mediated serine sensitivity shifts (Fig. 3*B*). This was evident for both a lock-ON (A413G) and a lock-OFF (A413T) lesion (*SI Appendix*, Fig. S1) at the same Tsr position, suggesting that a conformationally locked Tsr tip is immune to the signaling states of neighboring Tar receptors in shared core complexes.

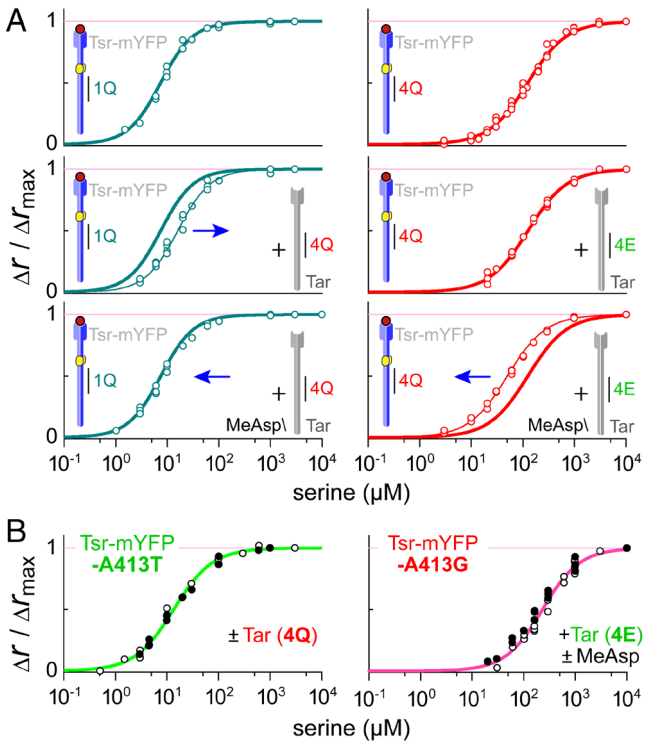

Fig. 3. Signaling interactions between Tar and Tsr receptors in mixed core complexes. (*A*) Dose-dependent anisotropy responses to serine measured in VF7 cells expressing Tsr-mYFP [QEEE] (1Q) (*Left* column) or Tsr-mYFP (4Q) (*Right* column), alone (*Top* row) or in combination with Tar (*Middle* row), or Tar plus 0.5 mM MeAsp (*Bottom* row). At least three and up to seven repetitions were done for each plot at different intermediate concentrations. Each dose–response plot was normalized to its maximal response, which depended on the mixing. Tsr expression was induced at 1.25 μM IPTG; Tar expression at 0.3 to 0.4 μM (4Q) or 0.75 μM (4E) NaSal. The thicker lines on each side are identical in all three plots (*Top* to *Bottom*) and serve as a reference. (*B*) Dose-dependent anisotropy responses measured as in (*A*). (*Left*) Tsr-mYFP/A413T (locked-OFF; see *SI Appendix*, Fig. S1) with (filled circles) or without (open circles) coexpressed Tar (4Q) receptors. (*Right*) Tsr-mYFP/A413G (locked-ON; see Fig. 2 and *SI Appendix*, Fig. S1) coexpressed with Tar (4E) with (filled circles) or without (open circles) MeAsp.

We also observed conformational communication between Tar and Tsr in mixed complexes by monitoring directly the anisotropy (homo-FRET) responses of tagged Tsr receptors to ligand binding by neighboring Tar receptors (Fig. 4). Mixing of untagged receptors with tagged receptors dilutes the mYFP tag in receptor complexes and therefore decreases overall the homo-FRET interactions, increases the fluorescence-anisotropy baseline, and reduces the response amplitudes (Fig. 4; see also *SI Appendix*, Fig. S4*A* for an assessment of the expression-levels). Nevertheless, binding of MeAsp to the Tar receptors led to an observable anisotropy response of the Tsr-mYFP receptors, hereafter referred to as "indirect" response (Fig. 4, arrows). The magnitude of the indirect responses is shown in *SI Appendix*, Fig. S4*B* as a function of Tar expression level. Notably, at the concentrations used in Figs. 3 and 4, a cross-response of Tsr to MeAsp (or aspartate) or Tar to serine was not observed by either anisotropy (32) or methylation rate (38) measurements. Here also, no response to MeAsp could be observed in cells expressing only Tsr-mYFP receptors (Fig. 4, black symbols), including the more serine-sensitive 4E or 1Q variants of Tsr-mYFP (*SI Appendix*, Fig. S4*C*). Thus, the indirect responses represent conformational changes affecting the tagged Tsr receptor that were triggered by MeAsp binding to their Tar neighbors.

Interestingly, the direction of the indirect response depended mainly on the signaling state of the tagged Tsr receptors rather than that of the Tar receptors that sense the MeAsp. In the case of highly active Tsr-mYFP (4Q) receptors, the indirect response to MeAsp was inverted in comparison to the direct response to serine (Fig. 4*B*, blue arrows; *SI Appendix*, Fig. S4 *B*, *Lower* plot). A similar inverted response had been previously noted in mixed receptor populations in cells lacking CheA and CheW, in which receptor trimers are less stable (39). In contrast, the indirect MeAsp response of low-activity Tsr-mYFP (4E) receptors was in the same direction as their direct response to serine (Fig. 4*A*, cyan arrows; *SI Appendix*, Fig. S4 *B*, *Upper* plot). Notably, the two Tar/Tsr-mYFP combinations result in different signaling interactions at the trimer tip (Fig. 4, *Right* diagrams). In both cases, binding of ligand to the untagged Tar receptors sends a strong OFF signal to their tips. However, with the adaptation domain of Tsr in a low-activity state (4E), the OFF state of the Tsr tip domains is reinforced by both internal and external coupling (Fig. 4*A*). In contrast, when the adaptation domain of Tsr is in a high-activity state (4Q), a conformational conflict between the interacting Tsr and Tar tip domains might be responsible for the inverted anisotropy response in the tagged Tsr reporters (Fig. 4*B*). The mechanism underlying that behavior remains to be determined.

The magnitude of the indirect responses (*SI Appendix*, Fig. S4*B*) may be influenced by several factors. On one hand, the more Tar receptors present in the cells, the more MeAsp sensors there are to communicate conformational signals to Tsr. On the other hand, due to dilution of the tagged Tsr, more untagged Tar receptors

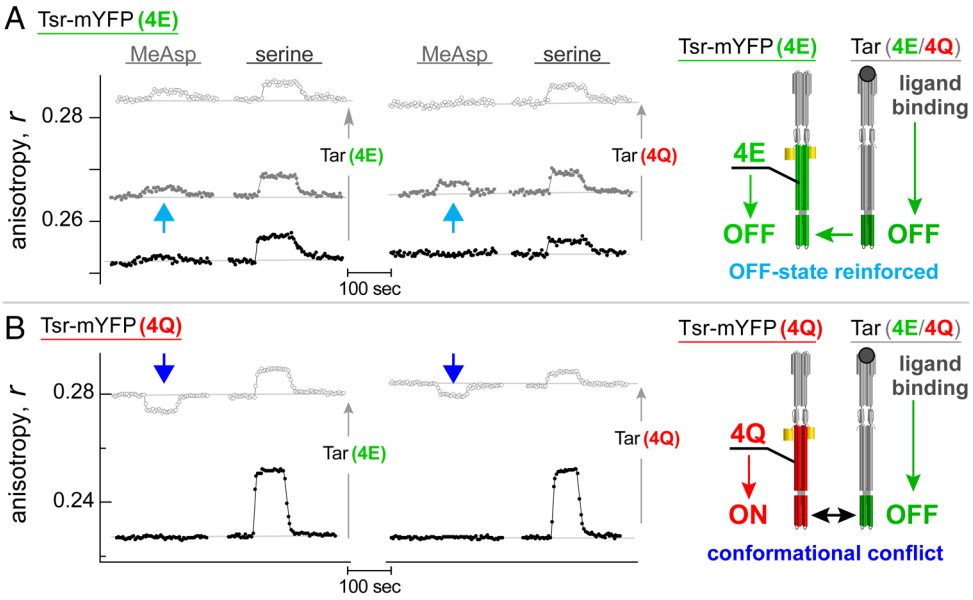

Fig. 4. Transmission of Tar ligand-binding signals to neighboring Tsr receptors. (*A*) Anisotropy responses measured in VF7 cells expressing Tsr-mYFP (4E) induced at 1.25 μM IPTG, either alone (black traces) or coexpressed with Tar (4E) or Tar (4Q), induced at 0.35 μM NaSal (dark gray traces) or 0.75 μM NaSal (light gray traces). (*B*) Anisotropy responses measured in VF7 cells expressing Tsr-mYFP (4Q) induced at 1.25 μM IPTG, either alone (black traces) or coexpressed with Tar (4E) or Tar (4Q), induced with 0.75 μM NaSal (light gray traces). Estimated Tar expression levels are shown in *SI Appendix*, Fig. S4*A*. Ligand responses were measured to serine (1 mM), which binds to the Tsr-mYFP receptors, or to MeAsp (1 mM), which binds to the untagged Tar receptors, as labeled. The dependence of the Tar-mediated indirect (MeAsp) responses of Tsr-mYFP (arrows) on Tar induction is shown in *SI Appendix*, Fig. S4*B*. Mechanistic interpretations of the opposing indirect responses in panels *A* and *B* (upward vs. downward arrows) based on tip interaction effects are shown on the *Right* (see text).

will reduce the resulting homo-FRET response. In addition, as demonstrated for example in Fig. 3*A*, the effective communication between Tar and Tsr may also depend on their signaling states.

Tip-locking lesions in Tsr-mYFP affected the indirect response to MeAsp in mixed receptor complexes. A locked-OFF lesion (A413T) at the tip of Tsr-mYFP blocked its indirect response to MeAsp mediated by Tar (4E), whereas a locked-ON lesion (A413G) still allowed an inverted response (Fig. 5 and *SI Appendix*, Fig. S5). This inverted response likely results from the strong conformational conflict between the locked-ON tip domain of Tsr (A413G) and the OFF-biased tip domain of MeAsp-bound Tar (see illustration in Fig. 4*B*). In contrast, a locked-ON (A411G) lesion in the tip of the untagged Tar receptors clearly blocked the inverted indirect response (Fig. 5 and *SI Appendix*, Fig. S5). Notably, the Tar-A411G

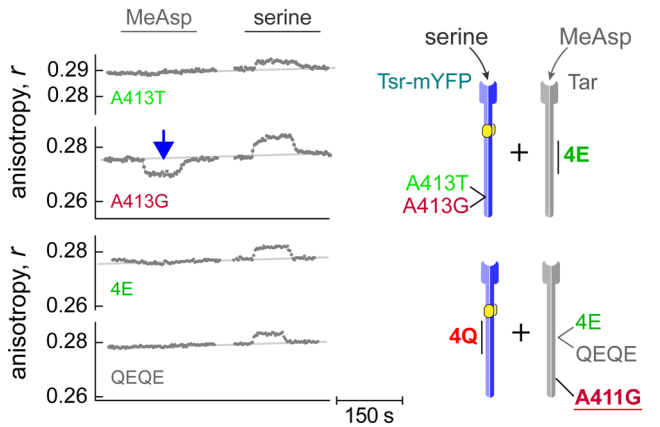

Fig. 5. The effect of locked-ON/OFF tip lesions on the indirect conformational responses in mixed complexes. Anisotropy responses measured in VF7 cells coexpressing Tsr-mYFP (induced at 1.25 μM IPTG) and untagged Tar (induced at 0.75 μM NaSal). Upper traces: Tsr-mYFP (QEQE) carried a locked-OFF (A413T) or locked-ON (A413G) tip lesion in combination with Tar (4E). Lower traces: Tsr-mYFP (4Q) in combination with Tar (4E) or Tar (QEQE), each bearing the locked-ON (A411G) tip lesion. The downward arrow indicates an indirect "inverted" conformational response. See *SI Appendix*, Fig. S5 for additional data.

receptor showed a clear anisotropy response to MeAsp (Fig. 2*B* and *SI Appendix*, Fig. S2), indicating conformational changes in their upper signaling domains. Therefore, the A411G lesion in Tar likely abolishes the inverted response in mixed trimers by locking the conformation of the Tar tip in the ON state, which prevents the conformational conflict with a Tsr tip that is also ON biased.

Ligand Dose-Dependence of Conformational vs. Kinase-Control Responses. We compared the full serine dose–response profiles of the FRET kinase assay at the hairpin tip with the corresponding membrane-proximal homo-FRET readout in Tsr-only signaling complexes (Fig. 6). The kinase and homo-FRET responses were similar overall and became more sensitive to ligand as the modification state shifted from 4Q (red symbols) to QEQE (blue symbols) and to 4E (green symbols). However, the dose–response behaviors differed, as the anisotropy (homo-FRET) responses were consistently more sensitive. Previous studies have shown that the kinase activity responses of receptor arrays (with native CheW) exhibit wider dynamic range compared with the receptor (anisotropy) responses in the absence of CheA/W altogether (32). Notably, these changes in dynamic range resulted from the fact that the low activity receptors (4E) became more sensitive upon networking but the highly active receptors (4Q) became less sensitive upon networking (9, 16, 32). In contrast, here, the conformational (anisotropy) responses of the receptors in core complexes were all shifted, to various degrees, toward lower concentrations relative to the integrated kinase activity responses in the same complexes (Fig. 6), possibly representing the internal coupling within core complexes.

Discussion

Signal Transmission through Individual Receptor Molecules. Chemoreceptor molecules have long been considered to operate as two-state signaling devices that switch between two distinct global states, corresponding to the kinase ON and OFF output states (14–16, 24, 25). This view implies that structural coupling

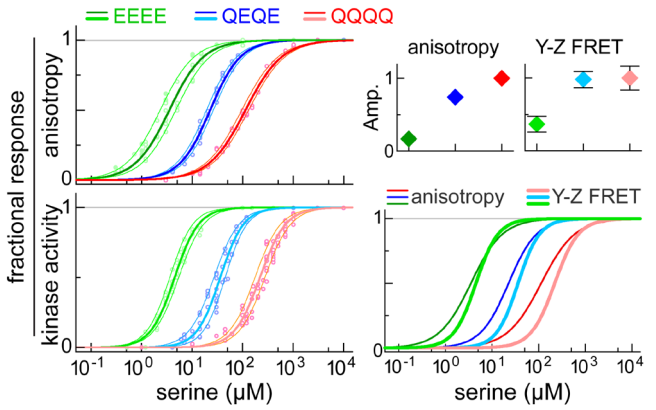

Fig. 6. Anisotropy and kinase-activity dose–responses in Tsr core complexes. Conformational (anisotropy) dose–responses were measured in VF7 cells expressing Tsr-mYFP in the (4E), (QEQE) and (4Q) modification states. Cells also harbored an empty pKG110 vector. Kinase activity (CheY-CheZ FRET) responses were measured in VF7 cells expressing Tsr-mCFP in (4E), (QEQE) and (4Q) modification states. Cells also expressed CheY-Z FRET pair from a pKG110 vector. The *Upper-Right* panel shows the relative response amplitudes at the three modification states. Thin lines define the range of potential fits at each modification state and the thick lines correspond to their average. The parameters for the average fits are ($K_{1/2}$/Hill coefficient): *Anisotropy*: 4E - 3.5/1.28, QEQE - 22.5/1.44, 4Q - 112.5/1.2; *Kinase activity*: 4E - 4.5/1.825, QEQE - 36/1.875, 4Q - 220/1.7. The *Lower Right* panel shows a comparison between the averaged kinase (thicker lines) and anisotropy (thinner lines) responses.

between successive domains is dominant over all other energies, such that the domains would be strictly correlated and the receptor dimers would function effectively as a two-state switch. However, our experiments with mYFP-tagged Tsr and Tar receptors locked in a kinase-ON output state revealed that the coupling energy between the upper signaling domains and the kinase-controlling hairpin tip must be rather moderate. The introduction of A413G/A411G lesions in the Tsr/Tar tips locked their output in a kinase-ON state (Fig. 2*A* and *SI Appendix*, Fig. S1). However, those tip lesions still allowed ligand-induced conformational (homo-FRET) responses in the upper signaling domain (Fig. 2*B* and *SI Appendix*, Fig. S2). In contrast, lesions in the upper domain of Tsr, I229A, or 5Q, which also locked tip output in a kinase-ON state (Fig. 2*A*), also affected the conformational (anisotropy) response to ligand (Fig. 2*B*). The region between the methylation sites and the tip domain is most notably demarcated by the glycine hinge and the flanking flexible regions (Fig. 1*B*) that may function as a coupling element (40, 41). These data indicate that, unlike a tightly coupled binary switch, ligand-induced conformational changes propagate through the signaling elements of a receptor dimer with a coupling energy that is not completely dominating the internal energies of its structural domains. A recent study of histidine-kinase receptors revealed a similar signaling property in PhoQ (42).

In principle, the upper receptor domain could influence the transition rates between the ON and OFF conformations of the tip domain, rather than its equilibrium bias, which would lead to asymmetric coupling between these domains. Such a mechanism has recently been suggested for the control of the kinase conformational state by the receptor tip domain (43). However, the observation that locking the tip domain in the ON state significantly alters the ligand sensitivity of the upper receptor domains (*SI Appendix*, Fig. S3) suggests that the coupling between the receptor domains occurs, at least in part, between their equilibrium bias.

Conformational Coupling between Receptors in Core Signaling Units. Receptor trimers of dimers are formed through direct and symmetric contacts between the tip regions of the dimers (Fig. 1*A*). However, at their outer tip interfaces, the contacts between each receptor dimer and the CheA/CheW proteins are asymmetric (Fig. 1 *A*, *Top* view): One receptor dimer contacts the P5 domain of CheA, one contacts the adapter protein CheW, and one makes no direct contact to either of them. Nonequivalent geometries might enable the members of a receptor trimer to play different roles in controlling core complex signaling activities (38); some receptors with primarily structural roles might not contribute directly to kinase control. However, we found here that core units containing both Tsr and Tar molecules exhibited signaling behaviors consistent with the presence of a conformational coupling between neighboring receptors through their tip domains. Such interactions shifted the serine sensitivity of Tsr anisotropy responses upon mixing with Tar receptors (Fig. 3) and produced Tsr conformational responses indirectly through their Tar partners (Fig. 4).

The trimer contact is the only recognized point of direct contact between dimers. In principle, effective coupling between dimers may also occur through membrane perturbations (44). However, given that locked-ON/OFF tip lesions could influence the coupling (Figs. 3 and 5), we suggest that the observed coupling mostly occurs through direct contacts between receptor tip domains. The observed coupling tended to bias neighboring tip domains to adopt a similar signaling state. Given such coupling between receptor tip domains, even if only one member of a trimer directly controls the kinase activity in a core unit, signals received by the other dimers can also influence kinase output.

A Model of Receptor Signaling Interactions in Core Complexes. Conformational coupling between the tip domains may be expected to yield a highly cooperative response of receptor trimers. However, limited internal coupling between successive receptor domains can offset this tendency. The behaviors observed here were therefore analyzed in the context of the following model for trimer signaling (Fig. 7*A*). To mimic the finite coupling between receptor domains, the model assumes that ligand binding initiates two distinguishable signaling responses in the receptor molecule: a primary conformational response in the upper (membrane-proximal) part and a secondary response at the kinase-controlling tip region. For simplicity, we treated the primary and tip regions as independent two-state elements with energy bias $\Delta E_{primary}$ and ΔE_{tip}. All energies here are normalized by temperature (k_BT). Consistent with the observation that Tsr tip fragments can readily activate the kinase (45), we assign an intrinsic ON bias to the tip domains ($\Delta E_{tip} < 0$). Ligand binding, characterized by the ligand affinities K_{on} and K_{off}, is coupled directly only to the ON and OFF conformational states related to the primary response, which is, in turn, coupled to the tip response with finite coupling energy (J_{intra}). In addition, consistent with the observations in Figs. 3–5, which suggested communication between neighboring dimers through their tip regions, we added a coupling energy (J_{tip}) between neighboring receptor tip domains that biases neighboring domains to adopt similar signaling states. The ligand-dependent ON probabilities of the two domains, $P_{primary}(L)$ and $P_{tip}(L)$, could be obtained as detailed in SI Model. Notably, if the coupling energies, J_{tip} and J_{intra}, are both taken to infinity, this model reverts back to the MWC model (*SI Appendix, SI Model*).

The following properties of this model are evident: The dose-dependent primary and tip responses can indeed be distinct (Fig. 7*B*, dashed and solid lines). Moreover, as shown in *SI Appendix*, Fig. S6*A*, if the anisotropy (homo-FRET) measurements correspond to $P_{primary}(L)$ and the kinase measurements to $P_{tip}(L)$, the model can reasonably reproduce the measured dose–responses behaviors observed in Fig. 6, although to a lesser extent for the Tsr(4E) kinase plot. In contrast to the view of the receptor as a two-state switch, which requires that the intradimer energy be much

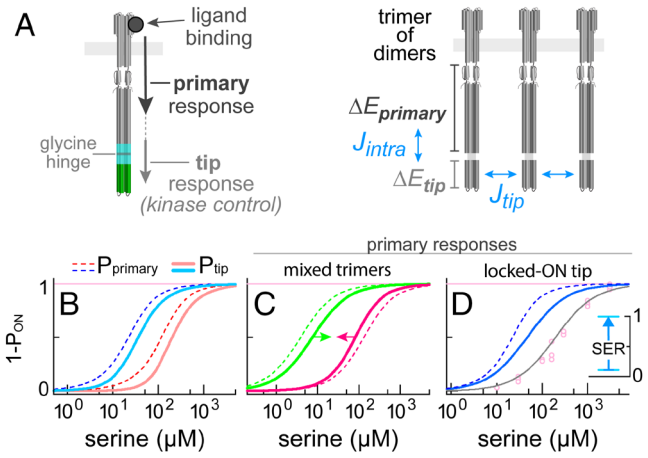

Fig. 7. A revised model for signaling in chemoreceptor trimers. (*A*) The model proposes that ligand-binding induces a primary response in the upper portion of receptor dimers that propagates to the receptor tip to control kinase output (see text for details). The energy biases of the primary ($\Delta E_{primary}$) and tip (ΔE_{tip}) responses are different and have a finite coupling energy (J_{intra}). In addition, neighboring receptor tips have a coupling energy (J_{tip}) that biases them to adopt similar signaling states. The ligand-dependent ON probabilities of the "primary" and "tip" regions, $P_{primary}(L)$ and $P_{tip}(L)$, respectively, were calculated as detailed in *SI Appendix, SI Model* section. The Tsr parameter values used here were derived from fitting the data (*SI Appendix*, Fig. S6*A*). (*B*) The inverted ON-probabilities $1\text{-}P_{primary}(L)$ (dashed lines) and $1\text{-}P_{tip}(L)$ (solid lines) are plotted for trimers with either QEQE or 4Q Tsr receptors. These plots demonstrate that the two regions can exhibit distinct response behaviors. (*C*) $1\text{-}P_{primary}(L)$ is plotted for Tsr (4E) trimers (green dotted lines) or similar trimers in which one receptor was replaced with an ON-biased Tar receptor that does not respond to serine, Tar ($\Delta E_{primary}$) = −2.4 (green solid lines). $1\text{-}P_{primary}(L)$ is also plotted for Tsr (4Q) trimers (red dotted lines) or similar trimers in which one receptor was replaced with a ligand-bound (OFF biased) Tar receptor, mimicked by setting Tar ($\Delta E_{primary}$) = 20 (red solid lines). These plots demonstrate that one receptor in a trimer can shift the responses of the other two receptors. (*D*) $1\text{-}P_{primary}(L)$ is plotted for trimers containing only Tsr(QEQE) receptors, either native (dotted blue line) or with locked-ON tip domain (solid blue line), mimicked by setting ΔE_{tip} = −20. The corresponding anisotropy dose–response measured with Tsr-mYFP/A413G is also shown (open circles), fitted (gray line) by assuming also a shift in $\Delta E_{primary}$ (−1.6) imposed by the locked-ON tip. The inset demonstrates a considerable shift in $P_{primary}(L)$ upon ligand binding in receptors with a locked-ON tip region (ΔE_{tip} = −20).

larger than all other energies, the intradimer coupling energy (J_{intra}) used here is comparable to other energies. Overall, larger J_{intra} leads to greater similarity between $P_{primary}(L)$ and $P_{tip}(L)$, which ultimately becomes identical when J_{intra} is fully dominant. On the other hand, smaller J_{intra} limits the ability of the upper receptor domains to compete with the intrinsic bias of the tip, strengthened by interdimer coupling, and thus limits the ability of ligand binding to fully stabilize the tip in the OFF state. Indeed, using the parameters detailed in *SI Appendix*, Fig. S6*A*, the predicted kinase inhibition was not complete (*SI Appendix*, Fig. S6*B*). However, this small but nonzero P_{tip} may also represent a weak nonlinear relation between P_{tip} and the actual kinase activity; see also refs. (38) and (46). Finally, the interdimer coupling (J_{inter}) is essential for having distinct $P_{primary}(L)$ and $P_{tip}(L)$ plots. Notably, in the absence of interdimer coupling, even with moderate J_{intra}, the normalized dose–response plots of $P_{primary}(L)$ and $P_{tip}(L)$ are still identical.

Second, consistent with the sensitivity shifts measured in mixed complexes (Fig. 3), a highly active receptor in a trimer (with $E_{primary} < 0$) shifts the dose–response of the other two low-activity receptors (with $E_{primary} > 0$) toward higher ligand concentrations (Fig. 7*C*, dashed and full green lines, respectively). In contrast, a ligand-bound receptor (with $E_{primary} \gg 1$) in a trimer shifts the dose–response of the other highly active receptors (with $E_{primary} < 0$) toward lower ligand concentrations (Fig. 7*C*, dashed and full red lines, respectively). Notably, the asymmetry between the Tsr(1Q) and Tsr(4Q) behaviors in Fig. 3*A* results from an asymmetry between the ON and OFF states related to the primary response, imposed by the ON bias of the tip.

Third, $P_{primary}$ readily responded to ligand even when the tip domain was locked-ON, mimicked by setting $E_{tip} \ll -1$ (Fig. 7 *D*, *Inset*). In addition, $P_{primary}$ became less sensitive to ligand upon locking the tip domain in the ON state (Fig. 7*D*, blue line). However, this sensitivity shift was smaller than the measured one (Fig. 7*D*, symbols). The measured sensitivity shift could be accounted for by allowing the tip to also influence the intrinsic energy bias of the primary response (Fig. 7*D*, gray line). However, such a change goes beyond the simple model considered here.

Overall, the combination of moderate coupling between successive domains within each receptor dimer, the inherent ON bias of the tip domains, and the coupling between neighboring tips leads to an asymmetry between the two receptor responses (Fig. 7*A*), which may lead to their distinct behaviors (Figs. 6 and 7). In essence, the independent responses of the upper domains are competing with the inherent ON bias of their tip domains reinforced by the direct coupling between the tips.

Inverted Coupling Effects. The "inverted" response occurs under conditions where the tips of neighboring dimers are strongly forced to adopt opposing signaling states (Fig. 4, blue arrow, and *SI Appendix*, Fig. S4*B*). Such conditions can be realized, for example, upon removal of high aspartate concentration. With aspartate present, adaptation tunes Tar receptors toward the 4Q state, while Tsr receptors remain closer to the 4E state. Thus, the removal of aspartate can transiently lead to a strong conflict. More broadly, such conflict can arise when cells navigate complex environments, where they experience, for example, a simultaneous increase in both attractant concentration detected by Tar and repellent concentration detected by Tsr.

The model outlined in Fig. 7*A* cannot account for this inverted response. In principle, the inverted responses could arise through dissociation of trimers and regrouping of the tagged receptors into Tsr-only trimers. This scenario is unlikely for two reasons: First, the signaling responses are clearly reversible. If regrouping of the tagged Tsr receptors occurred upon addition of MeAsp, there would be no reason for them to dissociate again upon its removal. Note that core complexes are stable, and a fast dissociation/association dynamic of these complexes does not appear to occur either in vivo (6) or in vitro (47). Moreover, one would expect that core complexes assembled with CheA and CheW would inhibit dissociation of trimers. However, the inverted response observed here was similar and even more pronounced than that previously reported in cells lacking the CheA and CheW proteins (39). Second, if mixed trimers were to dissociate when MeAsp is added, the Tar receptors could not affect the signaling state of the Tsr receptors (Fig. 3*A*).

We also note, however, that despite the ligand-induced downward (inverted) anisotropy response (Fig. 4*B*, blue arrows), the sensitivity shifts observed in Fig. 3 *A*, *Right-Lower* plot are consistent with an effective positive coupling between Tar and Tsr, which, in the presence of MeAsp, shifts the Tsr (4Q) receptors toward the OFF-state. Thus, under sharp conformational conflict between the tip domains of neighboring receptors in core complexes, the packing of the upper part of the receptors, above the glycine hinge, might be enhanced, while still adopting an intradimer helix-packing conformation that communicates an OFF signal to the receptor tip. Similarly, a locked-ON tip domain in Tsr prevents neighboring Tar receptors from influencing the signaling-related conformation of its upper domains and thus from shifting its ligand sensitivity (Fig. 3*B*), but still allows an inverted response (Fig. 5). Thus, the primary response itself may

not be restricted to two states, but rather may involve complex conformational changes (43). Moreover, under certain conditions, some aspects of these conformational changes may not directly control kinase output.

Overall, our data suggest a view of signaling in the core-complex in which moderate coupling exists between the signaling states of successive receptor domains and between neighboring receptor tip domains. Under these conditions, the trimer tip can act as a nuanced point of signal integration, where ligand-binding signals propagated along different dimers are integrated to mediate kinase control (38, 46). Networking of such complexes in large arrays would lead to additional coupling between them through direct signaling connections at the trimer-tip/CheA/CheW layer (Fig. 1*A*). Yet, the functioning of the trimer tip as a point of signal integration has clear implications for the manner in which signals are integrated in receptor arrays, including the dependence of signal integration on the overall receptor composition of the array and how these receptors are distributed within the array.

Materials and Methods

Bacterial Strains. Strain used in this study was *E. coli* K-12 strain RP437 (34) and its derivative VF7 [*cheW-X2* Δ(*tsr*) Δ(*aer*) Δ(*tap*) Δ(*trg*) Δ(*tar-cheZ*)] (13).

Plasmids. Plasmids used are listed in *SI Appendix*, Table S1. Genes encoding mYFP- or mCFP-tagged receptor variants were cloned in IPTG (isopropyl-b-D-thiogalactopyranoside)-regulatable expression vector pTrc99A (48), which confers resistance to ampicillin and uses the colE1 replication system. Genes encoding untagged Tar variants were cloned and expressed in sodium salicylate-regulatable expression vector pKG110 (49), which confers resistance to chloramphenicol and uses the p15A replication system.

Growth Conditions and Motility Buffer. Cell cultures were grown in tryptone broth (10 g/L tryptone, 5 g/L NaCl). For plasmid maintenance, chloramphenicol was used in tryptone broth at 25 μg/mL; ampicillin was used at 100 μg/mL. The motility buffer used in fluorescence anisotropy and FRET kinase experiments contained 10 mM potassium phosphate, 0.1 mM Ethylenediaminetetraacetic acid (EDTA), 1 μM methionine, 10 mM lactic acid, at pH 7.0.

Fluorescence Anisotropy Assays. VF7 cells carrying tagged-receptor expression plasmids were grown in 125 mL flasks filled with 10 mL tryptone broth plus appropriate antibiotics with shaking aeration at 33.5 °C to OD_{600} ~ 0.45. Cells were harvested by centrifugation, resuspended in motility buffer, and maintained at ~6 °C fridge until use. Tsr expression from pTrc99a derivatives was induced with 1.25 μM IPTG. Tar expression from compatible pKG110 plasmids was induced with Na salicylate (NaSal), as mentioned; for consistency, in experiments where only tagged receptors were expressed, cells carried the parental pKG110 vector. In vivo anisotropy experiments were performed at room temperature (21 to 22 °C) as previously described (32, 33, 36). In brief, cells were immobilized on a polylysine-coated coverslip, placed in a flow chamber, and mounted on a Nikon FN1 microscope. The mYFP fluorophore was excited with linearly polarized light, and the emitted fluorescence was split using a polarizing beam splitter cube into parallel (I_{par}) and perpendicular (I_{per}) polarizations, which were monitored using two photon counters. The steady-state polarization of the emitted fluorescence is represented here by the fluorescence anisotropy, *r*, defined as $(I_{par} - I_{per})/(I_{par} + 2 \cdot I_{per})$, where I_{per} has been corrected for imperfections in the optical system. Cells were tested for attractant responses by switching the flow chamber input to motility buffer containing serine, aspartate, or MeAsp; stimuli were reversed by switching the input flow back to motility buffer.

FRET-Based Kinase Assays. The in vivo kinase assay measures CheA activity-dependent interactions between CheY-mCherry and CheZ-mYFP expressed from a pKG110-based plasmid pAV109 (*SI Appendix*, Table S1) (12, 31). We used here a CheZ variant (CheZ-F98S) that has CheY-P phosphatase activity but does not associate with receptor complexes (50, 51). VF7 cells carrying pAV109 and a compatible pTrc99A-derived receptor plasmid were grown and harvested as for anisotropy experiments. Expression of the FRET reporter proteins was induced with 0.8 μM Na salicylate. As in the anisotropy experiments, cells were immobilized on a coverslip, placed in a flow chamber, and mounted on a Nikon FN1 microscope at room temperature (36). The mYFP donors were excited using unpolarized light, and fluorescence emission from the FRET donor and mCherry acceptor was continually monitored by photon-counting photomultipliers. Dose–response curves were obtained by plotting the fractional changes in kinase activity vs. the applied stimulus. Total CheA kinase activity was measured as the change elicited by a saturating stimulus or by 1 to 3 mM NaCN, which blocks cellular production of ATP, the phosphodonor for CheA autophosphorylation, leading to a FRET change that reflects the prechallenge CheA activity (35).

Protein Expression. VF7 cells expressing tagged Tsr, and untagged Tar receptors were grown in tryptone broth with appropriate antibiotics and inducers as for anisotropy and FRET kinase experiments. Cells were harvested by centrifugation and resuspended in 2× Laemmli sample buffer (52) at OD_{600} 4.5 and boiled for 5 min. The whole-cell lysates were analyzed by denaturing sodium-dodecyl-sulfate gel electrophoresis (10% polyacrylamide). Cells transferred to a polyvinylidene fluoride membrane using a wet blotter system. After blocking with 3% skim milk (Difco, BD Life Sciences) in Tris-buffered saline (added with 0.05% tween-20), receptor proteins were detected using an αTsr primary antibody, which reacts with both Tsr and Tar, at a 1:5,000 dilution, followed by an horseradish-peroxidase-conjugated secondary antibody (Jackson Immunoresearch) at a 1:10,000 dilution. Protein bands were visualized using an enhanced chemiluminescence kit, and densitometry analysis was done with ImageJ software.

Model. The probabilities of the primary and tip domains to be in the on state, $P_{primary}(L)$ and $P_{tip}(L)$, respectively (Fig. 7*A*) were calculated as: $P(L) = (\Sigma_i P^{on}{}_i \cdot e^{-E_i})/(\Sigma_i e^{-E_i})$, where *i* represents all possible trimer arrangements. See *SI Appendix, text* for details.

Data, Materials, and Software Availability. All study data are included in the article and/or *SI Appendix*.

ACKNOWLEDGMENTS. This work was supported by U.S. Public Health Service research grant GM19559 from the National Institute of General Medical Sciences (to J.S.P.), by the Israeli Foundation of Sciences and Humanities (to A.V.), and by research grant BSF 2017356 from the U.S.-Israel Binational Science Foundation (to J.S.P. and A.V.).

1. J. M. Keegstra, F. Carrara, R. Stocker, The ecological roles of bacterial chemotaxis. *Nat. Rev. Microbiol.* **20**, 491–504 (2022).
2. H. C. Berg, *E. coli in Motion* (Springer, NY, 2004).
3. R. P. Alexander, I. B. Zhulin, Evolutionary genomics reveals conserved structural determinants of signaling and adaptation in microbial chemoreceptors. *Proc. Natl. Acad. Sci. U.S.A.* **104**, 2885–2890 (2007).
4. J. S. Parkinson, G. L. Hazelbauer, J. J. Falke, Signaling and sensory adaptation in *Escherichia coli* chemoreceptors: 2015 update. *Trends Microbiol.* **23**, 257–266 (2015).
5. P. Ames, C. A. Studdert, R. H. Reiser, J. S. Parkinson, Collaborative signaling by mixed chemoreceptor teams in *Escherichia coli*. *Proc. Natl. Acad. Sci. U.S.A.* **99**, 7060–7065 (2002).
6. C. A. Studdert, J. S. Parkinson, Crosslinking snapshots of bacterial chemoreceptor squads. *Proc. Natl. Acad. Sci. U.S.A.* **101**, 2117–2122 (2004).
7. M. Li, G. L. Hazelbauer, Core unit of chemotaxis signaling complexes. *Proc. Natl. Acad. Sci. U.S.A.* **108**, 9390–9395 (2011).
8. A. Burt *et al.*, Complete structure of the chemosensory array core signalling unit in an *E. coli* minicell strain. *Nat. Comm.* **11**, 743 (2020).
9. G. E. Piñas, V. Frank, A. Vaknin, J. S. Parkinson, The source of high signal cooperativity in bacterial chemosensory arrays. *Proc. Natl. Acad. Sci. U.S.A.* **113**, 3335–3340 (2016).
10. J. Liu *et al.*, Molecular architecture of chemoreceptor arrays revealed by cryoelectron tomography of *Escherichia coli* minicells. *Proc. Natl. Acad. Sci. U.S.A.* **109**, E1481–E1488 (2012).
11. A. Briegel *et al.*, Bacterial chemoreceptor arrays are hexagonally packed trimers of receptor dimers networked by rings of kinase and coupling proteins. *Proc. Natl. Acad. Sci. U.S.A.* **109**, 3766–3771 (2012).
12. V. Sourjik, H. C. Berg, Receptor sensitivity in bacterial chemotaxis. *Proc. Natl. Acad. Sci. U.S.A.* **99**, 123–127 (2002).
13. V. Frank, G. E. Piñas, H. Cohen, J. S. Parkinson, A. Vaknin, Networked chemoreceptors benefit bacterial chemotaxis performance. *mBio* **7**, e01824-16 (2016).
14. Y. Tu, Quantitative modeling of bacterial chemotaxis: Signal amplification and accurate adaptation. *Annl. Rev. Biophys.* **42**, 337–359 (2013).
15. T. A. J. Duke, D. Bray, Heightened sensitivity of a lattice of membrane receptors. *Proc. Natl. Acad. Sci. U.S.A.* **96**, 10104–10108 (1999).
16. J. E. Keymer, R. G. Endres, M. Skoge, Y. Meir, N. S. Wingreen, Chemosensing in *Escherichia coli*: Two regimes of two-state receptors. *Proc. Natl. Acad. Sci. U.S.A.* **103**, 1786–1791 (2006).
17. V. Sourjik, H. C. Berg, Functional interactions between receptors in bacterial chemotaxis. *Nature* **428**, 437–441 (2004).
18. H. C. Berg, The rotary motor of bacterial flagella. *Annu. Rev. Biochem.* **72**, 19–54 (2003).

19. P. Dunten, D. E. Koshland, Tuning the responsiveness of a sensory receptor via covalent modification. *J. Biol. Chem.* **266**, 1491–1496 (1991).
20. H. C. Berg, P. M. Tedesco, Transient response to chemotactic stimuli in *Escherichia coli*. *Proc. Natl. Acad. Sci. U.S.A.* **72**, 3235–3239 (1975).
21. K. A. Borkovich, L. A. Alex, M. I. Simon, Attenuation of sensory receptor signaling by covalent modification. *Proc. Natl. Acad. Sci. U.S.A.* **89**, 6756–6760 (1992).
22. S. M. Block, J. E. Segall, H. C. Berg, Impulse responses in bacterial chemotaxis. *Cell* **31**, 215–226 (1982).
23. T. S. Shimizu, Y. Tu, H. C. Berg, A modular gradient-sensing network for chemotaxis in *Escherichia coli* revealed by responses to time-varying stimuli. *Mol. Sys. Biol.* **6**, 382 (2010).
24. S. Asakura, H. Honda, Two-state model for bacterial chemoreceptor proteins: The role of multiple methylation. *J. Mol. Biol.* **176**, 349–367 (1984).
25. J. A. Bornhorst, J. J. Falke, Evidence that both ligand binding and covalent adaptation drive a two-state equilibrium in the aspartate receptor signaling complex. *J. Gen. Physiol.* **118**, 693–710 (2001).
26. K. E. Swain, M. A. Gonzalez, J. J. Falke, Engineered socket study of signaling through a four-helix bundle: Evidence for a Yin–Yang mechanism in the kinase control module of the aspartate receptor. *Biochemistry* **48**, 9266–9277 (2009).
27. Q. Zhou, P. Ames, J. S. Parkinson, Biphasic control logic of HAMP domain signalling in the *Escherichia coli* serine chemoreceptor. *Mol. Microbiol.* **80**, 596–611 (2011).
28. Q. Zhou, P. Ames, J. S. Parkinson, Mutational analyses of HAMP helices suggest a dynamic bundle model of input-output signalling in chemoreceptors. *Mol. Microbiol.* **73**, 801–814 (2009).
29. V. Frank, A. Vaknin, Prolonged stimuli alter the bacterial chemosensory clusters. *Mol. Microbiol.* **88**, 634–644 (2013).
30. R. G. Endres *et al.*, Variable sizes of *Escherichia coli* chemoreceptor signaling teams. *Mol. Syst. Biol.* **4**, 211 (2008).
31. V. Sourjik, A. Vaknin, T. S. Shimizu, H. C. Berg, In vivo measurement by FRET of pathway activity in bacterial chemotaxis. *Methods Enzymol.* **423**, 365–391 (2007).
32. A. Vaknin, H. C. Berg, Physical responses of bacterial chemoreceptors. *J. Mol. Biol.* **366**, 1416–1423 (2007).
33. A. Vaknin, H. C. Berg, Osmotic stress mechanically perturbs chemoreceptors in *Escherichia coli*. *Proc. Natl. Acad. Sci. U.S.A.* **103**, 592–596 (2006).
34. J. S. Parkinson, S. E. Houts, Isolation and behavior of *Escherichia coli* deletion mutants lacking chemotaxis functions. *J. Bacteriol.* **151**, 106–113 (1982).
35. R.-Z. Lai, J. S. Parkinson, Functional suppression of HAMP domain signaling defects in the *E. coli* serine chemoreceptor. *J. Mol. Biol.* **426**, 3642–3655 (2014).
36. V. Frank, M. Koler, S. Furst, A. Vaknin, The physical and functional thermal sensitivity of bacterial chemoreceptors. *J. Mol. Biol.* **411**, 554–566 (2011).
37. M. Li, G. L. Hazelbauer, The carboxyl-terminal linker is important for chemoreceptor function. *Mol. Microbiol.* **60**, 469–479 (2006).
38. M. Li, G. L. Hazelbauer, Selective allosteric coupling in core chemotaxis signaling complexes. *Proc. Natl. Acad. Sci. U.S.A.* **111**, 15940–15945 (2014).
39. A. Vaknin, H. C. Berg, Direct evidence for coupling between bacterial chemoreceptors. *J. Mol. Biol.* **382**, 573–577 (2008).
40. A. Pedetta, D. A. Massazza, M. K. Herrera Seitz, C. A. Studdert, Mutational replacements at the "glycine hinge" of the *Escherichia coli* chemoreceptor Tsr support a signaling role for the C-helix residue. *Biochemistry* **56**, 3850–3862 (2017).
41. N. Akkaladevi, F. Bunyak, D. Stalla, T. A. White, G. L. Hazelbauer, Flexible Hinges in bacterial chemoreceptors. *J. Bacteriol.* **200**, e00593–17 (2018).
42. B. Mensa *et al.*, Allosteric mechanism of signal transduction in the two-component system histidine kinase PhoQ. *eLife* **10**, e73336 (2021).
43. D. Hathcock *et al.*, A nonequilibrium allosteric model for receptor-kinase complexes: The role of energy dissipation in chemotaxis signaling. *Proc. Natl. Acad. Sci. U.S.A.* **120**, e2303115120 (2023).
44. C. A. Haselwandter, N. S. Wingreen, The role of membrane-mediated interactions in the assembly and architecture of chemoreceptor lattices. *PLoS Comput. Biol.* **10**, e1003932 (2014).
45. P. Ames, Y. A. Yu, J. S. Parkinson, Methylation segments are not required for chemotactic signalling by cytoplasmic fragments of Tsr, the methyl-accepting serine chemoreceptor of *Escherichia coli*. *Mol. Microbiol.* **19**, 737–746 (1996).
46. B. A. Mello, W. Pan, G. L. Hazelbauer, Y. Tu, A dual regulation mechanism of histidine kinase CheA identified by combining network-dynamics modeling and system-level input-output data. *PLoS Comput. Biol.* **14**, e1006305 (2018).
47. X. Li, S. J. Eyles, L. K. Thompson, Hydrogen exchange of chemoreceptors in functional complexes suggests protein stabilization mediates long-range allosteric coupling. *J. Biol. Chem.* **294**, 16062–16079 (2019).
48. E. Amann, B. Ochs, K. J. Abel, Tightly regulated tac promoter vectors useful for the expression of unfused and fused proteins in *Escherichia coli*. *Gene* **69**, 301–315 (1988).
49. K. K. Gosink, M. del Carmen Burón-Barral, J. S. Parkinson, Signaling interactions between the aerotaxis transducer Aer and heterologous chemoreceptors in *Escherichia coli*. *J. Bacteriol.* **188**, 3487–3493 (2006).
50. A. Vaknin, H. C. Berg, Single-cell FRET imaging of phosphatase activity in the Escherichia coli chemotaxis system. *Proc. Natl. Acad. Sci. U.S.A.* **101**, 17072–17077 (2004).
51. B. J. Cantwell *et al.*, CheZ phosphatase localizes to chemoreceptor patches via CheA-short. *J. Bacteriol.* **185**, 2354–2361 (2003).
52. U. K. Laemmli, Cleavage of structural proteins during the assembly of the head of Bacteriophage T4. *Nature* **227**, 680–685 (1970).

Supplementary Information

Include:

SI Figures, including figure legends.

SI Model.

SI Table: Table S1.

Supplementary figure legends

Figure S1. **Kinase-control responses of mutant receptor core complexes**; **data complementary to the results in Fig. 2A.** Shown are traces of CheY-CheZ FRET signals (mCherry/mYFP fluorescence ratio) from VF7 cells expressing Tsr-mCFP receptors. Horizontal bars indicate ligand exposures (10 mM serine for Tsr; 10 mM MeAsp for Tar) and NaCN (1-3 mM) treatments. Three types of responses are illustrated: fully responding complexes (upper plot) show substantial and comparable responses to ligand and NaCN; locked-ON complexes (middle plots) show negligible ligand responses and substantial NaCN responses; and locked-OFF complexes (lower plot) show negligible ligand responses and only minor NaCN responses.

Figure S2. **Anisotropy (homo-FRET) responses of locked-ON receptor complexes; data complementary to the results in Fig. 2B.** Shown are anisotropy traces of mYFP-tagged Tsr or Tar receptors expressed in VF7 cells and challenged with 10 mM serine (dark gray bars) or MeAsp (light gray bars), respectively. Since the locked-ON lesions tended to lower the anisotropy baseline (less notable in the 5Q case), to permit direct comparison between the parental and mutant receptor responses the mutant traces were shifted upward and aligned with the parental traces. The horizontal lines and vertical brackets indicate the original averaged anisotropy baseline value and its variability across independent experiments. These traces also illustrate the effects of receptor signaling state on the homo-FRET baselines.

Figure S3. **Dose-response shifts in locked-ON receptors.** Dose-dependent anisotropy responses were measured from VF7 cells expressing Tsr-mYFP/A413G, Tar-mYFP/A411G, and their parent receptors. For Tsr-mYFP [QEQE], the grey line represents a fit to the data shown in Fig. 6. For Tar-mYFP [QEQE], the measured values (grey symbols) and fit line are shown. For Tar-mYFP/A411G, both MeAsp (open green symbols) and the 12-fold more potent Asp (filled green symbols) were tested, effectively extending the range of ligand concentrations (the Asp X-axis values were adjusted accordingly). Note that the larger shift in Tar sensitivity correlates with a larger shift in the baseline anisotropy shown in Fig. S2.

Figure S4. **Protein abundance and 'indirect' response amplitudes; data complementary to the results in Fig. 4.** Experiments were done with VF7 cells expressing Tsr-mYFP (1.25 μM IPTG induction) and untagged Tar receptors (induced at three different inducer concentrations: 0, 0.35, and 0.75 μM Na Sal). (**A**) Protein expression was analyzed by SDS-PAGE and immunoblotting with an anti-Tsr antibody that recognizes epitopes in the conserved hairpin tip regions of both Tsr and Tar (see Materials and Methods for additional experimental details). Data for several independent measurements with both Tar (4Q) and Tar (4E) are combined. Note that total receptor expression level ranged from 60-120% of the native chromosomally expressed Tar+Tar amount in wild-type RP437 cells. (**B**) Binding of ligand to the untagged Tar receptors triggers an indirect anisotropy response measured from the neighboring Tsr-mYFP receptors (see Fig. 4). The amplitudes of these responses to MeAsp (1 mM) are shown here as a function of Tar inducer concentration, [NaSal]. Data are shown for four receptor combinations: *Upper plot* – Tsr-mYFP (4E) coexpressed with either Tar(4E) (green) or Tar(4Q) (red). *Lower plot* – Tsr-mYFP (4Q) coexpressed with either Tar(4E) (green) or Tar(4Q) (red). Lines are a guide to the eye. (**C**) Anisotropy responses to either serine (blue bars) or MeAsp (grey bars) were measured in VF7 cells expressing Tsr-mYFP (4E or 1Q) and an empty Tar plasmid (pKG110). Serine and MeAsp concentrations were both either 1 mM (4E receptors) or 0.5 mM (1Q receptors), corresponding to experiments presented in Figs. 4 and 3, respectively. Note that there was no cross response of Tsr to MeAsp in the absence of Tar.

Figure S5. **Additional examples of direct and indirect homo-FRET responses in mixed complexes; data complementary to the results in Fig. 5.** Anisotropy responses to either 1 mM serine (blue bars) or 1 mM MeAsp (grey bars) were measured in VF7 cells coexpressing various combinations of Tsr-mYFP (induced at 1.25 μM IPTG) and untagged Tar (induced at 0.75 μM NaSal).

Figure S6. **Fitting the data with the model**. (**A**) The data presented in Fig. 6 (symbols) are fitted by the model described in Fig. 7 (lines, SI model). The probability of the primary domain to be in the ON state, $P_{primary}(L)$, was fitted to the anisotropy data (right plot) and the probability of the tip domain to be in the ON state, $P_{tip}(L)$, was fitted to the kinase data (left plot). To match the plotted data (Fig. 6), the probabilities were normalized as follows:

$$\text{plotted lines: } 1 - [P_{on}(L) - P_{on}(sat.)] / [P_{on}(0) - P_{on}(sat.)]$$

where L is the ligand concentration and $P_{on}(sat.)$ is the probability at saturating ligand concentration. The probabilities in the absence of serine, $P_{on}(0) - P_{on}(sat.)$, corresponding to the measured response amplitudes, are plotted in the inset. The model parameters used here were: $\Delta E_{primary}$= -1.76 (4Q), -0.2 (QEQE), or +2.6 (4E), and ΔE_{tip}=-1.5; J_{intra}=2.2 and J_{tip}=2; K_{on}= 10 mM and K_{off}= 5 μM. (**B**) The non-normalized $P_{tip}(L)$ is plotted as a function of ligand (serine) concentration for the same parameter values as in (A). Note that $P_{tip}(sat.)$ is not zero and remains approximately 0.12. This may suggest a weak non-linear relation between $P_{tip}(L)$ and the actual kinase activity, which seems to be fully inhibited.

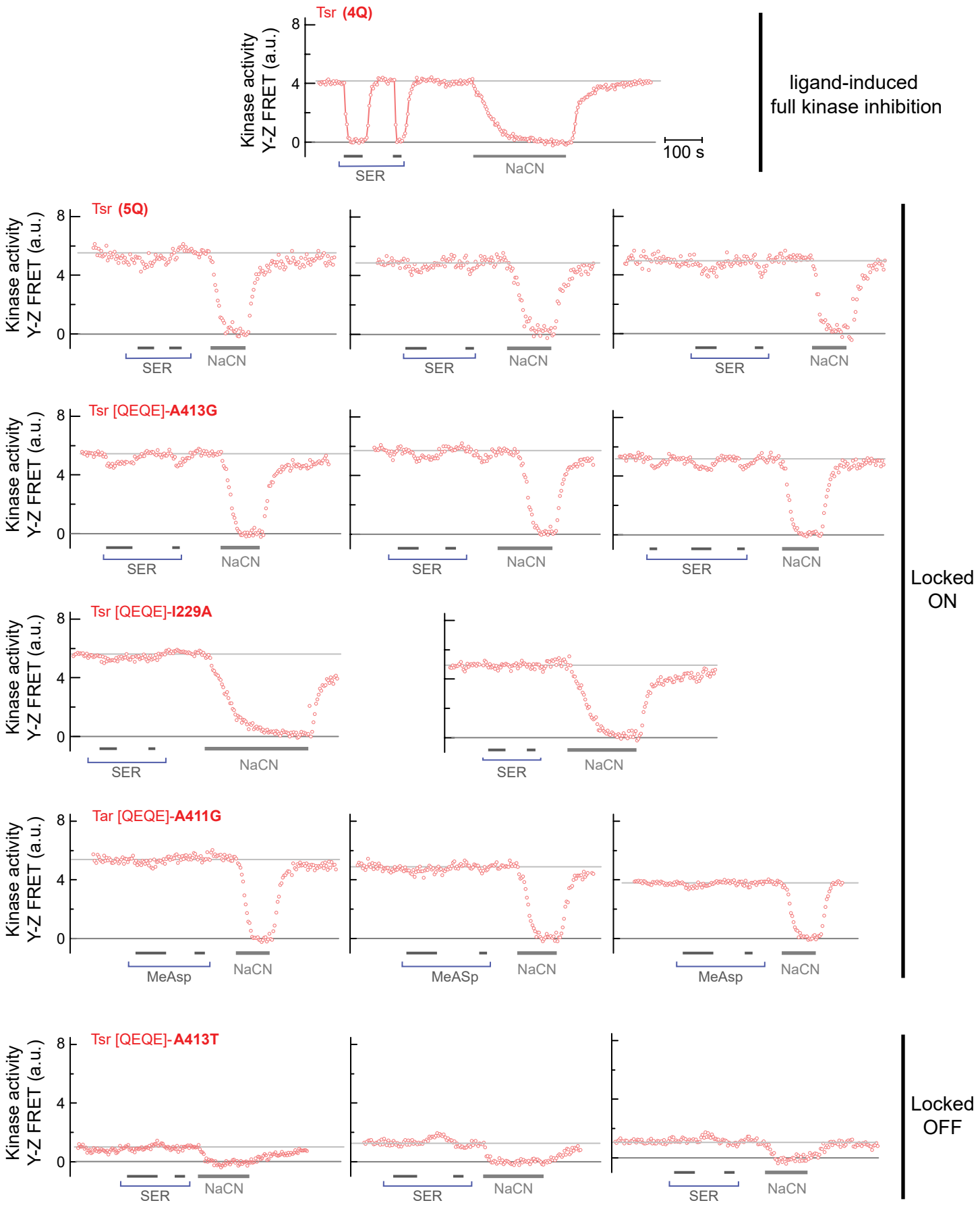
Tsr (4Q)
Kinase activity
Y-Z FRET (a.u.)
8
4
0
100 s
SER
NaCN
ligand-induced
full kinase inhibition
Tsr (5Q)
Tsr [QEQE]-A413G
Tsr [QEQE]-I229A
Tar [QEQE]-A411G
MeAsp
MeASp
Locked
ON
Tsr [QEQE]-A413T
Locked
OFF

Figure S1

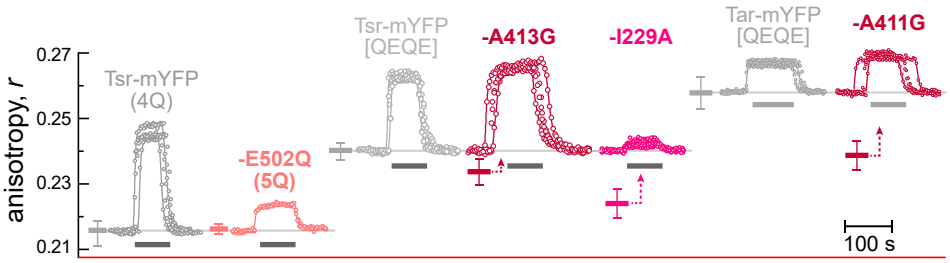
anisotropy, r
0.27
0.25
0.23
0.21
Tsr-mYFP
(4Q)
-E502Q
(5Q)
Tsr-mYFP
[QEQE]
-A413G
-I229A
Tar-mYFP
[QEQE]
-A411G
100 s

Figure S2

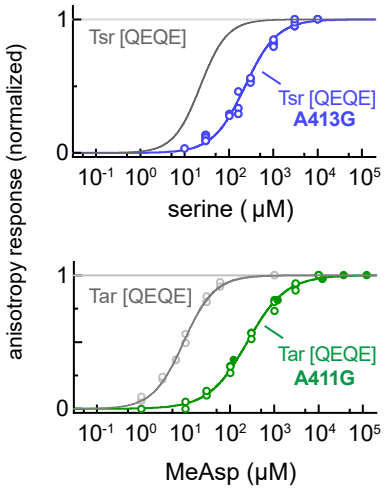
anisotropy response (normalized)
1
0
Tsr [QEQE]
Tsr [QEQE]
A413G
10-1 100 101 102 103 104 105
serine (μM)
1
0
Tar [QEQE]
Tar [QEQE]
A411G
10-1 100 101 102 103 104 105
MeAsp (μM)

Figure S3

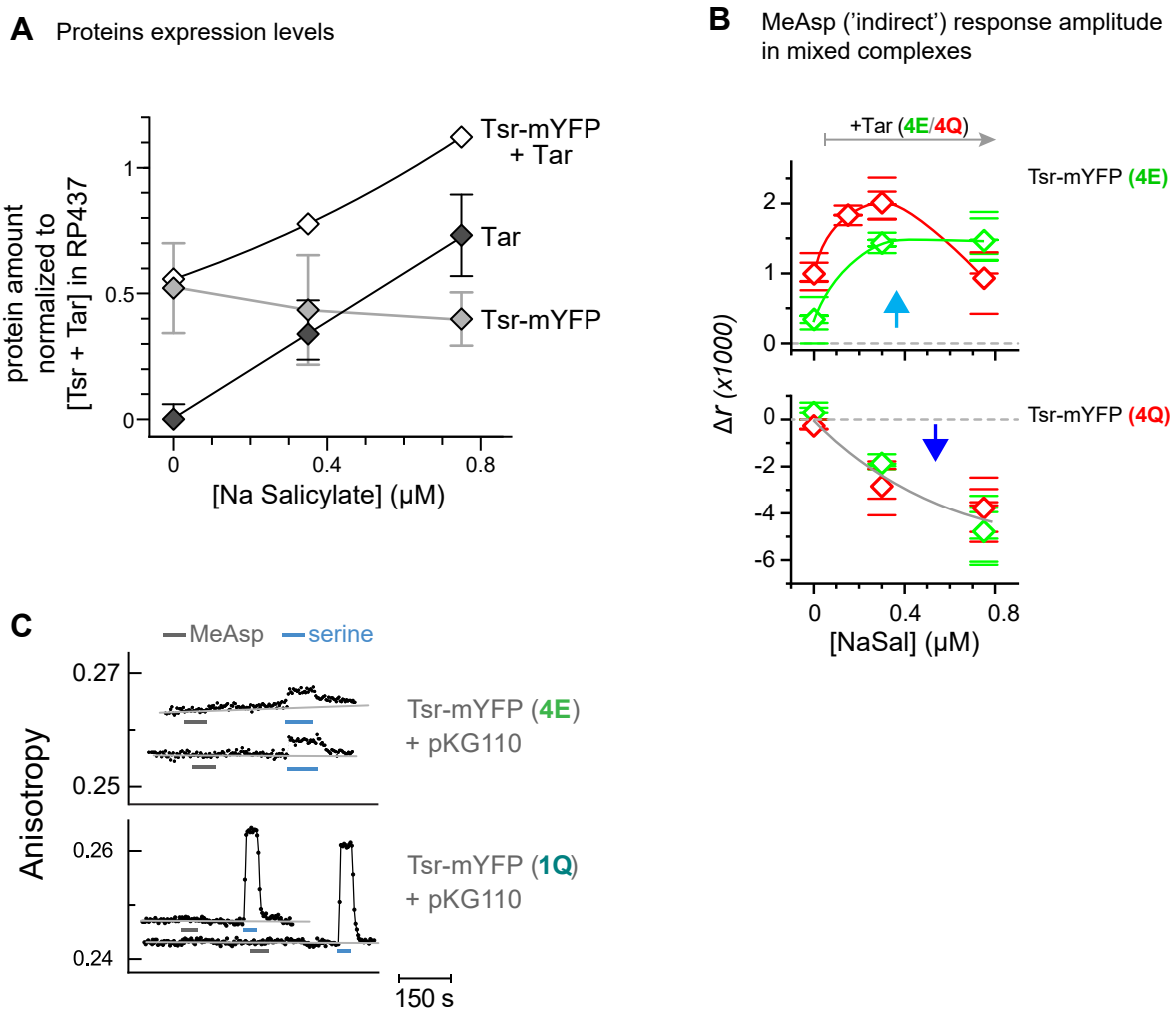
A
Proteins expression levels
protein amount
normalized to
[Tsr + Tar] in RP437
Tsr-mYFP
+ Tar
Tar
Tsr-mYFP
[Na Salicylate] (μM)
B
MeAsp ('indirect') response amplitude
in mixed complexes
+Tar (4E/4Q)
Tsr-mYFP (4E)
Tsr-mYFP (4Q)
Δr (x1000)
[NaSal] (μM)
C
MeAsp
serine
Anisotropy
Tsr-mYFP (4E)
+ pKG110
Tsr-mYFP (1Q)
+ pKG110
150 s

Figure S4

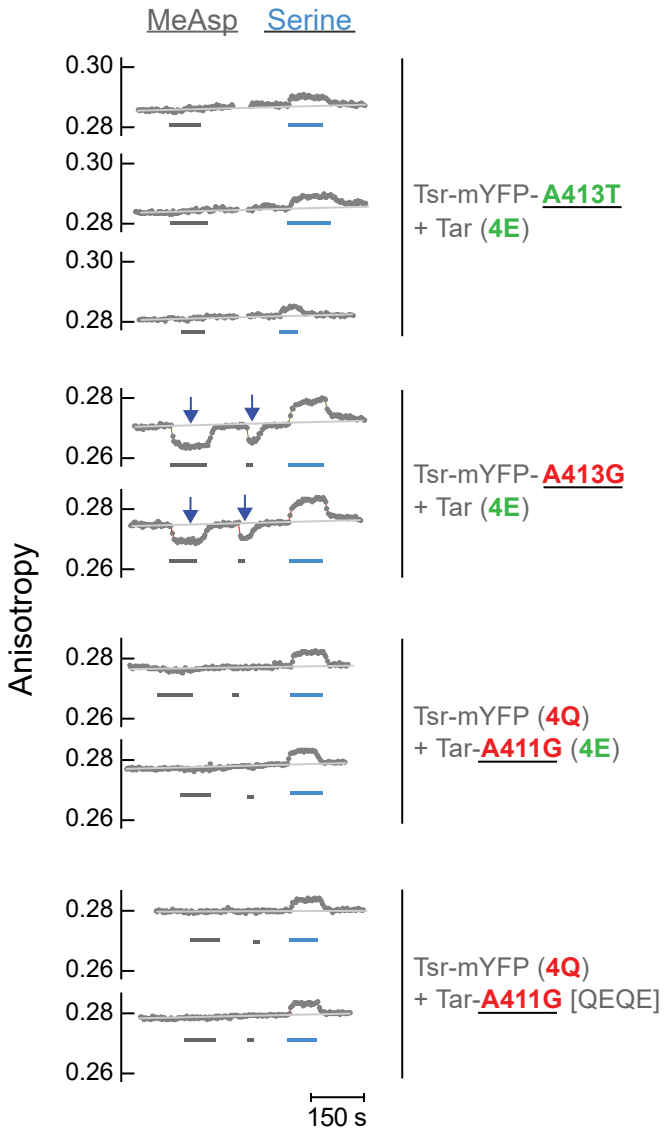
MeAsp
Serine
Anisotropy
0.30
0.28
0.26
Tsr-mYFP-A413T
+ Tar (4E)
Tsr-mYFP-A413G
+ Tar (4E)
Tsr-mYFP (4Q)
+ Tar-A411G (4E)
Tsr-mYFP (4Q)
+ Tar-A411G [QEQE]
150 s

Figure S5

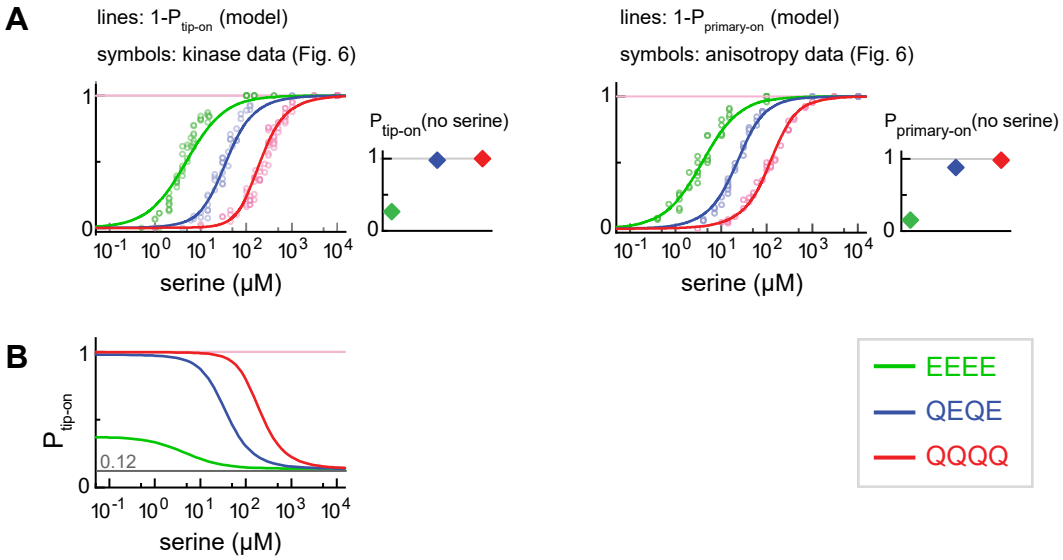
A
lines: 1-P tip-on (model)
symbols: kinase data (Fig. 6)
P tip-on (no serine)
serine (μM)
lines: 1-P primary-on (model)
symbols: anisotropy data (Fig. 6)
P primary-on (no serine)
serine (μM)
B
P tip-on
0.12
serine (μM)
EEEE
QEQE
QQQQ

Figure S6

Supplementary text - **Model solution**

The model considered here for trimer signaling is described in Fig. 7A. Each receptor dimer is assumed to have a 'primary' and 'tip' domain with finite coupling energy between them. Each of the domains is considered as a two-state (on/off) switch with corresponding energies:

Primary domain:	E_{on}^{p} and E_{off}^{p}	and	$\Delta E_p \equiv E_{on}^{p} - E_{off}^{p}$
Tip domain:	E_{on}^{t} and E_{off}^{t}	and	$\Delta E_t \equiv E_{on}^{t} - E_{off}^{t}$

And, the coupling energy between the primary and tip domains is J_{intra}, hereafter labelled J_r

In addition, we assume interdimer positive coupling between neighboring tip domains J_{tip} , hereafter labelled J_t

Part A – The probability that the primary domain adopts the ON conformation – $P_{primary-ON}$ is given by:

$$P_{primary-ON} = \frac{\sum(P^{on})_i \cdot e^{-E_i}}{Z} \qquad with \quad Z = \sum_i e^{-E_i} = \sum(P^{on})_i \cdot e^{-E_i} + \sum(P^{off})_i \cdot e^{-E_i}$$

And therefor

$$(Eq.1) \qquad P_{primary-ON} = \frac{\sum(P^{on})_i \cdot e^{-E_i}}{Z} = \frac{\sum(P^{on})_i \cdot e^{-E_i}}{\sum(P^{on})_i \cdot e^{-E_i} + \sum(P^{off})_i \cdot e^{-E_i}} = \frac{1}{1 + \frac{Z - \sum(P^{on})_i \cdot e^{-E_i}}{\sum(P^{on})_i \cdot e^{-E_i}}}$$

where $(P^{on})_i$ and $(P^{off})_i$ represent the expected value of P^{on} and P^{off} in the state i, and E_i is the energy of that state. A concise presentation of these summations is shown below.

Since the primary domain is directly coupled to ligand binding, in each state (on/off) it could be either unbound, with no additional energy, or bound by ligand with an additional energy $\ln(L/K_{on/off})$.

We therefor defined the following constants:

$$a \equiv e^{-E_{off}^{p}}\left(1 + \frac{L}{K_{off}}\right) \quad \text{and} \quad b \equiv e^{-E_{on}^{p}}\left(1 + \frac{L}{K_{on}}\right)$$

Such that if consider only the primary domains:

$$\sum_i e^{-E_i} = a^3 + 3a^2b + 3ab^2 + b^3$$

However, for each combination of the primary domains, the summation in Eq. 1 includes also the combinations of the tip domains with their respective energies, which includes the coupling energies J_{intra} and J_{tip} .

We therefor defined the following constants:

Primary domains

$A_t \equiv e^{-3E_{off}^t} \cdot \{1 + 3e^{-\Delta E_t} \cdot (e^{-J_r}) \cdot e^{-2J_t} + 3e^{-2\Delta E_t} \cdot (e^{-2J_r}) \cdot e^{-2J_t} + e^{-3\Delta E_t} \cdot (e^{-3J_r})\}$ All '*off* '

$B_t \equiv e^{-3E_{off}^t} \cdot \{e^{-J_r} + e^{-\Delta E_t} \cdot (1 + 2e^{-2J_r}) \cdot e^{-2J_t} + e^{-2\Delta E_t} \cdot (2e^{-J_r} + e^{-3J_r}) \cdot e^{-2J_t} + e^{-3\Delta E_t} \cdot (e^{-2J_r})\}$ 2 *off*, 1 *on*

$C_t \equiv e^{-3E_{off}^t} \cdot \{e^{-2J_r} + e^{-\Delta E_t} \cdot (2e^{-J_r} + e^{-3J_r}) \cdot e^{-2J_t} + e^{-2\Delta E_t} \cdot (1 + 2e^{-2J_r}) \cdot e^{-2J_t} + e^{-3\Delta E_t} \cdot (e^{-J_r})\}$ 1 *off*, 2 *on*

$D_t \equiv e^{-3E_{off}^t} \cdot \{e^{-3J_r} + 3e^{-\Delta E_t} \cdot (e^{-2J_r}) \cdot e^{-2J_t} + 3e^{-2\Delta E_t} \cdot (e^{-J_r}) \cdot e^{-2J_t} + e^{-3\Delta E_t}\}$ All '*on*'

Such that the partition function can be then written as:

$$Z = \sum_i e^{-E_i} = a^3 \cdot A_t + 3a^2 b \cdot B_t + 3ab^2 \cdot C_t + b^3 \cdot D_t$$

And,

$$\sum (P^{on})_i \cdot e^{-E_i} = 0 \cdot a^3 \cdot A_t + (1/3) \cdot 3a^2 b \cdot B_t + (2/3) \cdot 3ab^2 \cdot C_t + 1 \cdot b^3 \cdot D_t$$

$$Z - \sum (P^{on})_i \cdot e^{-E_i} = a^3 \cdot A_t + 2 \cdot a^2 b \cdot B_t + ab^2 \cdot C_t$$

Thus, using the expressions described above, *Eq.1* can be written as:

$$P_{primary-ON} = \frac{1}{1 + \frac{a^3 \cdot A_t + 2a^2 b \cdot B_t + ab^2 \cdot C_t}{a^2 b \cdot B_t + 2ab^2 \cdot C_t + b^3 \cdot D_t}} = \frac{1}{1 + \frac{a \cdot \{a^2 \cdot A_t + 2ab \cdot B_t + b^2 \cdot C_t\}/b^2}{b \cdot \{a^2 \cdot B_t + 2ab \cdot C_t + b^2 \cdot D_t\}/b^2}}$$

And finally,

$$P_{primary-ON} = \frac{1}{1 + \eta \cdot \frac{\eta^2 \cdot A_t + 2\eta \cdot B_t + C_t}{\eta^2 \cdot B_t + 2\eta \cdot C_t + D_t}} \qquad with \qquad \eta \equiv \frac{a}{b} = e^{\Delta E_p} \cdot f(L)$$

$$f(L) \equiv \frac{(1 + L/K_{off})}{(1 + L/K_{on})}$$

Part B – The probability that the tip domain to adopt the ON conformation – P_{tip-ON}

As before,

$$Eq.2 \qquad P_{tip-ON} = \frac{\sum(P^{on})_i \cdot e^{-E_i}}{Z} \qquad with \quad Z = \sum_i e^{-E_i} = \sum(P^{on})_i \cdot e^{-E_i} + \sum(P^{off})_i \cdot e^{-E_i}$$

Now, for each state (on/off) of the tip domain, the primary domain can be in either in the on or off start, which, in turn, can be either unbound, with no additional energy, or bound by ligand with an additional energy $\ln(L/K_{on/off})$.

Thus, we now defined the quantities *a* and *b*, which describes individual dimers, as follows:

$$a \equiv e^{-E^t_{off}} \cdot \left\{ e^{-E^p_{off}} \cdot \left(1 + \frac{L}{K_{off}}\right) + e^{-(E^p_{on}+J_r)} \cdot \left(1 + \frac{L}{K_{on}}\right) \right\} \qquad \text{tip '}\textit{off}\text{'}$$

$$b \equiv e^{-E^t_{on}} \cdot \left\{ e^{-(E^p_{off}+J_r)} \cdot \left(1 + \frac{L}{K_{off}}\right) + e^{-E^p_{on}} \cdot \left(1 + \frac{L}{K_{on}}\right) \right\} \qquad \text{tip '}\textit{on}\text{'}$$

However, for each combination of the tip domains the coupling between them (J_r) should also be considered, and thus, the partition function can be written as:

$$Z = \sum_i e^{-E_i} = a^3 + 3a^2b \cdot e^{-2J_t} + 3ab^2 \cdot e^{-2J_t} + b^3$$

And,

$$\sum(P^{on})_i \cdot e^{-E_i} = 0 \cdot\ a^3\ + (1/3) \cdot 3a^2b \cdot e^{-2J_t} + (2/3) \cdot 3ab^2 \cdot e^{-2J_t} + 1 \cdot b^3 = a^2b \cdot e^{-2J_t} + 2ab^2 \cdot e^{-2J_t} + b^3$$

$$Z - \sum(P^{on})_i \cdot e^{-E_i} = a^3 + 2a^2b \cdot e^{-2J_t} + ab^2 \cdot e^{-2J_t}$$

And thus, again, using the expressions described above, *Eq. 2* can be written as:

$$P_{tip-ON} = \frac{1}{1 + \frac{a^3 + 2a^2b \cdot e^{-2J_t} + ab^2 \cdot e^{-2J_t}}{a^2b \cdot e^{-2J_t} + 2ab^2 \cdot e^{-2J_t} + b^3}} = \frac{1}{1 + \frac{(a/b)^3 + 2(a/b)^2 \cdot e^{-2J_t} + (a/b) \cdot e^{-2J_t}}{(a/b)^2 \cdot e^{-2J_t} + 2(a/b) \cdot e^{-2J_t} + 1}}$$

And finally,

$$P_{tip-ON} = \frac{1}{1 + \delta^3 \cdot \frac{1 + (2\delta^{-1} + \delta^{-2}) \cdot e^{-2J_t}}{1 + (\delta^2 + 2\delta) \cdot e^{-2J_t}}} \qquad with \qquad \delta \equiv \frac{a}{b} = e^{\Delta E_t} \cdot \frac{e^{-J_r} + e^{\Delta E_p} \cdot f(L)}{1 + e^{\Delta E_p - J_r} \cdot f(L)}$$

$$f(L) \equiv \frac{(1 + L/K_{off})}{(1 + L/K_{on})}$$

Part C – The MWC limit

The MWC model assumes that each dimer, as a whole, act as a 'two-state' switch and thus corresponds to infinite internal coupling

$$\boldsymbol{J_r \rightarrow infinity}$$

Which leads to $A_t \rightarrow 1$

$B_t \rightarrow e^{-\Delta E_t} \cdot e^{-2J_t}$

$C_t \rightarrow e^{-2\Delta E_t} \cdot e^{-2J_t}$

$D_t \rightarrow e^{-3\Delta E_t}$

$\eta \rightarrow e^{\Delta E_p} \cdot f(L)$

$\delta \rightarrow e^{\Delta E_p + \Delta E_t} \cdot f(L) = e^{\Delta E} \cdot f(L) \quad ; \quad \Delta E \equiv \Delta E_p + \Delta E_t$

And, as expected,

$$\boldsymbol{P_{primary-ON}} \rightarrow \frac{1}{1+\eta \cdot \frac{\eta^2 + 2\eta \cdot e^{-\Delta E_t} \cdot e^{-2J_t} + e^{-2\Delta E_t} \cdot e^{-2J_t}}{\eta^2 \cdot e^{-\Delta E_t} \cdot e^{-2J_t} + 2\eta \cdot e^{-2\Delta E_t} \cdot e^{-2J_t} + e^{-3\Delta E_t}}}$$

$$= \frac{1}{1+\eta \cdot \frac{\eta^2 \cdot \{1 + (2\eta^{-1} \cdot e^{-\Delta E_t} + \eta^{-2} \cdot e^{-2\Delta E_t}) \cdot e^{-2J_t}\}}{e^{-3\Delta E_t} \cdot \{1 + (\eta^2 \cdot e^{2\Delta E_t} + 2\eta \cdot e^{\Delta E_t}) \cdot e^{-2J_t}\}}}$$

$$= \frac{1}{1+[e^{\Delta E_p + \Delta E_t} \cdot f(L)]^3 \cdot \frac{1 + \{2[e^{\Delta E_p + \Delta E_t} \cdot f(L)]^{-1} + [e^{\Delta E_p + \Delta E_t} \cdot f(L)]^{-2}\} \cdot e^{-2J_t}}{1 + \{[e^{\Delta E_p + \Delta E_t} \cdot f(L)]^2 + 2[e^{\Delta E_p + \Delta E_t} \cdot f(L)]^1\} \cdot e^{-2J_t}}}$$

$$= \frac{1}{1+[e^{\Delta E} \cdot f(L)]^3 \cdot \frac{1 + \{2[e^{\Delta E} \cdot f(L)]^{-1} + [e^{\Delta E} \cdot f(L)]^{-2}\} \cdot e^{-2J_t}}{1 + \{[e^{\Delta E} \cdot f(L)]^2 + 2[e^{\Delta E} \cdot f(L)]^1\} \cdot e^{-2J_t}}}$$

$$= \frac{1}{1+\delta^3 \cdot \frac{1 + \{2\delta^{-1} + \delta^{-2}\} \cdot e^{-2J_t}}{1 + \{\delta^2 + 2\delta\} \cdot e^{-2J_t}}} \quad = \boldsymbol{P_{tip-ON}}$$

The MWC model further assumes that the coupling between dimers is infinite. Thus,

Setting, $\boldsymbol{J_t \rightarrow infinity}$

We get,

$$\boldsymbol{P_{primary/tip}} \rightarrow \frac{1}{1+\delta^3 \cdot \frac{1+0}{1+0}} = \frac{1}{1+\{e^{\Delta E} \cdot f(L)\}^3}$$

which is indeed the MWC result for N=3.

Part D – Mixed trimers.

The solid lines in Fig. 7C were calculated along the lines described above (parts A and B) except that one receptor in the trimer considered 'Tar', namely, it was not coupled to ligand. This 'Tar' receptor assumed to have similar properties as the 'Tsr' (ligand responding) receptors: similar internal coupling (J_{intra}); similar inherent tip bias (ΔE_{tip}); and, similar tip coupling energy to the 'Tsr' receptors (J_{tip}). However, it could have a distinct 'adaptation modifications', namely, distinct primary domain bias ($\Delta E_{primary}$), specified in the figure legend.

Table S1. Plasmids

plasmid	properties / expressed receptor insert	reference
group 1	pTrc99A derivatives; confer ampicillin resistance; colE1 replication system; IPTG-inducible expression	{amann, 1988}
pAV44	Tar [1-527/QEQE]-mYFP	{frank, 2011}
pAV55	Tsr [1-520/QEQE]-mYFP	{frank, 2011}
pAV73	Tsr [1-520/EEEE]-mYFP	{frank, 2011}
pAV74	Tsr [1-520/QQQQ]-mYFP	{frank, 2011}
pAV88	Tsr [QQQQ]-mYFP	this study
pAV163	Tsr [1-520/QQQQ]-mCFP	this study
pAV404	Tsr [1-520/QEQE]-mYFP/A413G	this study
pAV405	Tsr [1-520/QEQE]-mYFP/A413T	this study
pAV406	Tsr [1-520/QEQE]-mCFP/A413G	this study
pAV447	Tar-mCFP/A411G	this study
pAV450	Tsr [1-520/EEEE]-mCFP	this study
pAV451	Tsr [1-520/QEQE]-mCFP	this study
pAV452	Tar [1-527/QEQE]-mYFP/A411G	this study
pAV454	Tsr [1-520/QEEE]-mYFP	this study
pAV460	Tsr [1-520/QQQQ]-mYFP/E502Q	this study
pAV461	Tsr [1-520/QQQQ]-mCFP/E502Q	this study
group 2	pKG110 derivatives; confer chloramphenicol resistance; p15A replication system; sodium salicylate-inducible expression	{gosink, 2006}
pAV109	CheY-mCherry/CheZ-YFP/F98S	{frank, 2011}
pAV138	Tar [EEEE]	this study
pAV139	Tar [QQQQ]	{frank, 2016}
pAV275	Tar [QEQE]/A411T	this study
pAV431	Tar [EEEE]/A411G	this study
pAV432	Tar [EEEE]/A411T	this study
pAV437	Tar [QEQE]/A411G	this study